Clinical Science (2018) **132** 2241–2259
https://doi.org/10.1042/CS20180662

PORTLAND PRESS

Research Article

Degranulation of gastrointestinal mast cells contributes to hepatic ischemia–reperfusion injury in mice

Zhigang He[1,*], Yue Li[2,*], Sunqiang Ma[1], Muqing Yang[1], Yuanyuan Ma[1], Cheng Ma[1], Jian Song[1], Tianyu Yu[1], Siqi Zhang[3] and Jiyu Li[1]

[1]Department of General Surgery, Shanghai Tenth People's Hospital School of Medicine, Tongji University, 301 Middle Yanchang Road, Shanghai 200072, P.R. China; [2]Department of Obstetrics and Gynecology, Shanghai Tenth People's Hospital School of Medicine, Tongji University, 301 Middle Yanchang Road, Shanghai 200072, P.R. China; [3]Department of Cardiology, Jiangsu Province Hospital, Medical School of Nanjing University, Nanjing 210029, P.R. China

Correspondence: Jiyu Li (leejiyu@sina.com)

OPEN ACCESS

The pathological changes following liver damage, including those caused by ischemia and reperfusion (I/R), are closely related to gastrointestinal dysregulation. Mast cells (MCs) are tissue-resident immune cells abundant in the gastrointestinal system that play diverse roles. In view of the characteristic localization of MCs around the microvasculature, we hypothesized that a stimulus-specific set of mediators released through degranulation of gastrointestinal MCs, which are enriched in hepatic sinusoids via the hepatic system, subsequently participate in associated pathological development within the liver. To elucidate the biological role of gastrointestinal MC granules in liver damage, we employed an experimental liver I/R model that allows conditional ablation of MCs. Marked degranulation was detected during I/R, which showed a significant positive correlation with liver damage. Our experiments further disclosed that MC degranulation primarily enhanced the cycle of inflammatory damage in I/R liver consisting of liver sinusoidal endothelial cell death, neutrophil infiltration, and formation of a neutrophil extracellular trap, with a concomitant increase in adhesion molecules, inflammatory cytokines, chemokines, and oxidative stress. Based on the collective results, we propose that suppression of activity or number of MCs may present an effective strategy for protection against hepatic I/R injury.

Introduction

Organ injury, driven by transient ischemia followed by reperfusion (I/R), is a common complication in a number of diseases such as stroke, myocardial infarction, vascular surgery, and organ transplantation. In the clinical setting, liver I/R injury usually occurs during organ transplantation, surgical removal of hepatic tumors or trauma and hemorrhagic circulatory shock, accounting for ∼10% of early graft failures and increased prevalence of chronic rejection or even death [1]. Liver I/R injury actually represents a continuum of exogenous antigen-independent inflammatory processes including inflammatory cell activation, immune cell regulation, cytokine release, and oxidant attack, ultimately leading to hepatocyte and endothelial cell death. Effective treatment of hepatic I/R injury is a major clinical challenge, and a major research focus is clarification of the relevant mechanisms underlying hepatic I/R with a view to optimize and innovative delivery of current clinical interventions [2].

Mast cells (MCs) are tissue-based stationary effector cells that present first-line defense against various challenges as they are closely related to the inflammatory injury process [3]. The specific role of MCs during I/R in different tissues and organs has been of increasing interest to researchers in recent years [4-6]. However, the relationship between MCs and hepatic I/R injury remains to be elucidated.

[*] These authors contributed equally to this work.

Received: 29 July 2018
Revised: 01 October 2018
Accepted: 08 October 2018

Accepted Manuscript Online: 09 October 2018
Version of Record published: 29 October 2018

© 2018 The Author(s). This is an open access article published by Portland Press Limited on behalf of the Biochemical Society and distributed under the Creative Commons Attribution License 4.0 (CC BY-NC-ND).

Clinical Science (2018) **132** 2241–2259
https://doi.org/10.1042/CS20180662

MCs are derived from precursor cells in the bone marrow and mature under the influence of the stem cell factor, c-kit ligand, with the final phenotype being dependent on the microenvironment of residence. To exert specific effects, MCs release granules upon activation, which contain preformed histamine, cytokines, and specific proteases (such as chymase and tryptase). Immediately after degranulation, MCs synthesize various *de novo* inflammatory cytokines, chemokines, lipid mediators, and growth factors. However, the mechanisms by which MCs interact with other leukocytes to mediate inflammation or tissue injury are unknown at present [7]. In addition, MCs regulate vascular function and pathological changes by contacting independent and dependent mechanisms based on their capacity to produce a series of soluble factors that are distributed around blood vessels [8].

MCs are functionally much more diverse than previously understood and implicated in the pathogenesis of several types of I/R injury. In mouse models of myocardial infarction, the extent of tissue damage is correlated with MC degranulation, following which MC protease 4 antagonizes prosurvival signaling to promote cell death and adverse cardiac remodeling days after infarction [9]. Moreover, MC deficiency or pharmacologic inhibition in mice leads to a less severe phenotype after injury to the gut [10]. During renal I/R, MCs have been shown to play a deleterious role in the acute inflammatory phase, promoting subsequent fibrosis development [11]. However, there are some studies, as well, report no differences in the degree of organ injury in relation to the presence of MCs in mice [12].

Unlike other organs, the liver has a dual blood supply system involving the hepatic artery and portal vein that mainly collect blood from the spleen, stomach, intestine, and mesentery. The portal vein blood flow contains several nutrients and biological mediators from the gastrointestinal tract, which are crucial for maintaining the normal morphology and function of the liver. In previous studies, only rats within the rodent group were utilized as research subjects for hepatic I/R-associated MCs due to the presence of very few MCs in mouse liver [13,14]. However, the mouse gastrointestinal tract is rich in MCs, which may be related to its host defense function [15]. The gastrointestinal hyperemia and its barrier dysfunction represent the important systemic features during liver I/R injury [16], and the activation of gastrointestinal MCs and further their influence on liver injury at a distance via the vena portae should be evaluated. In particular, we speculate that granulated mediators or specific MC-related products are transported to liver sinusoids via the blood circulation and thus in direct contact with liver sinusoidal endothelial cells (LSECs), suggesting a close association between gastrointestinal MCs and liver I/R injury.

One of the main challenges of using mouse models for determining the roles of MCs in human liver pathology is that the number and distribution of these cells differ between laboratory mice and humans. $Kit^{W\text{-}sh/W\text{-}sh}$ mice lack MCs in all sites while wild-type $Kit^{+/+}$ C57BL/6 mice contain MCs primarily in gastrointestinal and skin tissues with few amounts in the liver [17]. Considering the distribution patterns of MCs in wild-type $Kit^{+/+}$ C57BL/6 mice, these animals present an excellent tool for evaluating the role of gastrointestinal MCs in liver I/R damage. Furthermore, MCs have been detected following intravenous injection of wild-type bone marrow-derived cultured mast cells (BMMCs) into MC-deficient Kit $^{W\text{-}sh/W\text{-}sh}$ mice in a C57BL/6 background. Adoptive reconstitution with BMMC transfer into Kit $^{W\text{-}sh/W\text{-}sh}$ mice (Kit $^{W\text{-}sh/W\text{-}sh}$ RMC mice) suggests the possibility of 'humanizing' mice with respect to MC diversity [18,19]. To establish the role of gastrointestinal MCs in murine hepatic I/R, we constructed a partial (70%) warm I/R injury model using the experimental mice described above. Our experiments disclosed that MCs are activated during the process of gastrointestinal congestion and recanalization. Following reperfusion, the degree of liver injury in wild-type C57BL/6 and MC-reconstituted Kit $^{W\text{-}sh/W\text{-}sh}$ mice was more severe, compared with that in Kit $^{W\text{-}sh/W\text{-}sh}$ mice. We additionally demonstrated that MC degranulation boosts the cycle of inflammatory damage in I/R liver consisting of LSEC death, neutrophil infiltration, and formation of neutrophil extracellular trap (NET), concomitant with increased numbers of proinflammatory cytokines, chemokines, adhesion molecules, and oxidative stress. Given that aggravated inflammatory injury of liver tissue is correlated with gastrointestinal MC activation, we propose that impairment of MC activity and/or suppression of MC numbers may present an effective strategy for protection against hepatic I/R injury.

Materials and methods

Reconstitution of Kit $^{W\text{-}sh/W\text{-}sh}$ mice with BMMCs and ethics statement

For *in vivo* studies, wild-type (C57BL/6 Kit $^{+/+}$) and MC-deficient (C57BL/6 Kit $^{W\text{-}sh/W\text{-}sh}$) mice were utilized. C57BL/6 Kit $^{+/+}$ mice were purchased from Shanghai Laboratory Animal Co Ltd. (SLAC, Shanghai, China), and Kit $^{W\text{-}sh/W\text{-}sh}$ mice from Jackson Laboratories (Bar Harbor, ME, U.S.A.). BMMCs were prepared by differentiating bone marrow cells in IL-3 and stem cell factor. BMMC adoptive transfer, termed the 'mast cell knock-in' approach [18], was performed using 4- to 6-week-old male Kit $^{W\text{-}sh/W\text{-}sh}$ mice via tail vein injection (two injections of 5×10^6 cells per mouse). Only male mice were used and strains matched by age and body weight. All animal experiments were conducted with

© 2018 The Author(s). This is an open access article published by Portland Press Limited on behalf of the Biochemical Society and distributed under the Creative Commons Attribution License 4.0 (CC BY-NC-ND).

the approval of the Local Ethics Committee responsible for regulating animal research in Tongji University, with animal care performed strictly according to the guidelines for the care and use of laboratory animals published by the US National Institutes of Health (NIH Publication No.85-23, revised 1996).

Model of partial hepatic I/R injury

We employed a well-established mouse model of partial warm hepatic I/R injury. Briefly, mice were anesthetized with sodium pentobarbital (60 mg/kg, i.p.). A midline laparotomy was performed, and an atraumatic clip was used to interrupt blood supply to the left lateral and median lobes of the liver. Evidence of ischemia was confirmed by visualization of pale blanching of ischemic lobes. The peritoneum was closed, and mice were placed on a heating pad (∼37°C). The ambient temperature ranged between 25 and 26°C. After 60 min of partial hepatic ischemia, the clip was removed to initiate hepatic reperfusion. Sham control mice underwent the same surgical procedure without vascular occlusion. Mice were humanely killed after the indicated periods of reperfusion, and blood as well as samples of the left lateral lobe, stomach and intestine obtained for analysis.

Liver damage assessment

Blood was obtained via cardiac puncture, and serum was isolated. To assess liver function and cellular injury following liver I/R, serum alanine aminotransferase (ALT) and aspartate aminotransferase (AST) levels were measured using the automated chemistry analyzer (OLYMPUS AU1000; Olympus, Tokyo, Japan). Liver tissues (cephalad lobes) were fixed in neutral buffered formalin, embedded in paraffin, and sections (5 μm) stained with hematoxylin and eosin (H&E) for histological analysis. The severity of liver I/R injury was graded blindly using *Suzuki's* criteria on a scale from 0 to 4. Samples with no necrosis, congestion, or centrilobular ballooning were given a score of 0 while severe congestion and > 60% lobular necrosis were assigned a value of 4. In addition, endothelial dysfunction was scored as follows: 0, absent; 1, mild endothelial dysfunction; 2, severe endothelial dysfunction; 3, 2 + infiltration of regenerating endothelial cells and inflammatory cells; and 4, 3 + vascular stenosis. For assessing the oxidation–reduction status of liver, the malondialdehyde (MDA) level was measured via the thiobarbituric acid method using liver homogenates. MDA detection was conducted according to the manufacturer's instructions with the aid of commercial kits (Nanjing Jiancheng Biological Institute, Jiangsu, China) and concentrations expressed as nanomoles per milligram of protein.

RNA isolation and quantitative real-time PCR

Total RNA was extracted from frozen liver using the RNeasy Mini Kit (Qiagen, Valencia, CA, U.S.A.) according to the manufacturer's instructions. A Nanodrop spectrophotometer (NanoDrop Technologies, Wilmington, DE, U.S.A.) was used to measure the total RNA concentration, and the quality assessed based on 260/280 and 230/260 ratios. In total, 5 μg RNA was reverse-transcribed into cDNA with a PrimeScript RT Master Mix (Takara Bio Inc., Otsu, Japan) and relative gene expression determined using the Roche LightCycler 480 SYBR Green system (Roche, Rotkreuz, Switzerland). Alternatively, semi-quantitative RT-PCR was performed and the amplification products analyzed via agarose gel electrophoresis. Target gene expression was calculated in relation to that of the reference gene *GAPDH*. The specific primers employed are presented in Supplementary Table S1.

Histological analysis of MCs

To identify MCs in mice, immunofluorescence and histochemical staining with toluidine blue were performed on 5 μm sections of routinely prepared paraffin-embedded tissues. For immunofluorescence staining, sections were washed three times with PBS after a 5 min high-pressure antigen retrieval process in sodium citrate buffer (100×, pH 6.0) and blocked with PBS containing 10% goat serum at room temperature. Monoclonal mouse antibody against mast cell tryptase (1:100; Abcam, Cambridge, MA, U.S.A.) was used as the primary antibody and anti-mouse IgG Fab2 (1:500; CST, Cell Signaling Technology Inc., Boston, MA, U.S.A.) as the secondary antibody. Finally, preparations were washed with PBS and mounted in fluorescent mounting medium with DAPI (Invitrogen, Camarillo, CA, U.S.A.). Negative controls were processed in the same manner but without the primary antibody. For toluidine blue staining (Sigma, St. Louis, MO, U.S.A.), slides were rinsed with PBS for 10 min and stained with 0.5% w/v toluidine blue (Sigma) in 0.5 N HCl (Baker, Philipsburg, NJ, U.S.A.) for 30 min.

MCs were identified based on the ability of granules to exhibit metachromatic staining. Quantitative analysis of MC density in organs was performed by counting the number of tryptase-positive and toluidine blue-positive MCs in 10 non-overlapping high-powered fields (HPFs) (40×) under a confocal laser scanning microscope (Carl Zeiss AG, Jena, Germany). MC density was expressed as cells/mm^2. To count the number of degranulated mast cells and

© 2018 The Author(s). This is an open access article published by Portland Press Limited on behalf of the Biochemical Society and distributed under the Creative Commons Attribution License 4.0 (CC BY-NC-ND).

Clinical Science (2018) **132** 2241–2259
https://doi.org/10.1042/CS20180662

assess the correlations between degranulation factors and liver injury, images obtained from high-throughput digital pathology section scanner were analyzed using Case Viewer.

Flow cytometry analysis

Cells isolated from the tissues of interest were incubated in the dark at 4°C for 30 min with the antibody mix. Briefly, single resuspended cells were prepared in wash buffer containing PBS with 0.1% sodium azide. Antibodies specific for respective cell markers were diluted in the appropriate volumes of FACS buffer containing 1% BSA and incubated with cells for 30 min at 4°C. After washing twice with FACS buffer, cells were fixed with IC Fixation Buffer (eBioscience**,** San Diego, CA, U.S.A.) for 20 min at room temperature, followed by permeabilization with Perm (eBioscience). Antibodies specific for cellular markers were diluted to the appropriate volume in Perm. Incubations were performed in the dark and flow cytometric data acquired using a FACS Calibur flow cytometer (BD Biosciences, San Jose, CA, U.S.A.), followed by analysis using FlowJo software (Treestar, Ashland, OR, U.S.A.). The following antibodies were used: APC-conjugated CD11b (BD Biosciences), PerCP/CyTM5.5-conjugated CD45 (BD Biosciences), FITC-conjugated FcεRIα (BioLegend, San Diego, CA, U.S.A.), PE-conjugated CD117/c-Kit (BioLegend), APC-conjugated F4/80 (BioLegend), FITC-conjugated Stabilin-2 (Bioss, Beijing, China), and FITC-conjugated Ly6G (BD Biosciences). We defined MCs as CD45+CD11b- FcεRIα+CD117/c-Kit+; LSECs as F4/80-Stabilin-2+; and infiltrating neutrophils as CD45+CD11b+Ly6G+. In addition, apoptosis of LSECs was evaluated using the PE-Annexin V/7-ADD apoptosis detection kit (BD Biosciences) according to the manufacturer's instructions. Each experiment was repeated a minimum of three times.

Measurements of histamine, tryptase, adhesion molecules, cytokines, myeloperoxidase, and NET formation

Blood samples were drawn into serum separation tubes and serum aliquots stored at −80°C until analysis. Serum histamine (SPI-Bio, Bertin Pharma, France) and tryptase (LS-Bio Seattle, WA, U.S.A.) were measured using a competitive enzyme immunoassay. The levels of the soluble biomarkers vascular cell adhesion molecule 1 (VCAM-1), intercellular adhesion molecule 1 (ICAM-1), TNF-α, MCP-1, thromboxane B2 (TxB2) (R&D Systems, Minneapolis, MN, U.S.A.), and 6-keto-prostaglandin F1α (6-keto-PgF1α) (Cayman chemical, Michigan, U.S.A.) were assessed with commercially available ELISA kits. Equal volumes of each sample were loaded according to the instructions for individual kits. Levels were quantitatively determined based on standard curves and presented as picograms per milliliter. Neutrophil sequestration within the liver was quantified by measuring tissue myeloperoxidase (MPO) activity as described previously. Briefly, tissue samples were homogenized in 20 mM phosphate buffer (pH 7.4) and centrifuged at 4°C for 10 min at ∼10000×$\boldsymbol{g}$. The pellets obtained were resuspended in 50 mM phosphate buffer (pH 6.0) containing 0.5% hexadecyltrimethylammonium bromide, subjected to three cycles of freezing and thawing and further disrupted via sonication (40 s). Following centrifugation of samples for 5 min at 4°C at 10000×$\boldsymbol{g}$, the supernatant fractions were used for the MPO assay. Aliquots of supernatant (50 μl) were incubated in a solution consisting of 1.6 mM tetramethylbenzidine, 80 mM sodium phosphate buffer, and 0.3 mM hydrogen peroxidase at 37°C for 110 s, following which the reaction was terminated with 2 M H_2SO_4 and absorbance recorded at 450 nm. The results were adjusted for protein concentration and MPO activity expressed as units per gram of protein (U/g). One Antibody array (AAM-CYT-G2, RayBiotech, Norcross, GA) was further used to detect some interesting cytokines. To quantify NET DNA in mouse serum, a PicoGreen assay kit (Invitrogen, San Diego, CA, U.S.A.) was utilized according to the manufacturer's instructions. Serum levels of Cit-H3, another specific marker of NET formation, were measured using the Cayman's Cit-H3 ELISA kit for mouse.

Apoptosis and necrosis assays

TUNEL staining was performed using the *In Situ* Cell Death Detection Kit (Roche Applied Science) according to the manufacturer's instructions. Microscopic quantification analyses were performed in 10 HPFs per specimen at a magnification of 400×. For additional confirmation, a set of cell death markers (caspase 3/7 activity, DNA fragmentation, poly (ADP-ribose) polymerase (PARP) activity) was detected after 24 h of reperfusion (I/R 24 h). Caspase 3/7 activity in hepatic tissue lysates was measured using the Apo-One Homogenous Caspase-3/7 assay kit (Promega Corp., Madison, WI, U.S.A.). Quantitative determination of cytoplasmic histone-associated DNA fragmentation (mono- and oligonucleosomes) due to cell death in liver homogenates was performed using an ELISA kit (Roche Diagnostics Corp., Indianapolis, IN, U.S.A.). PARP enzyme activity was quantified with the PARP universal colorimetric assay kit (R&D Systems Ltd., Abingdon, U.K.), following the manufacturer's instructions.

© 2018 The Author(s). This is an open access article published by Portland Press Limited on behalf of the Biochemical Society and distributed under the Creative Commons Attribution License 4.0 (CC BY-NC-ND).

Immunohistochemistry

Immunohistochemical analysis was performed primarily to determine the number of neutrophils and expression levels of inflammatory cytokines in liver. Formalin-fixed pancreas sections were deparaffinized in xylene and rehydrated through a graded ethanol series followed by treatment with 3% hydrogen peroxide for 10 min to inactivate endogenous peroxidase, and subsequently washed with PBS for 5 min. After microwave antigen retrieval, sections were washed in PBS and blocked in 10% normal serum with 1% BSA in TBS for 2 h at room temperature. Sections were incubated overnight at 4°C with Gr-1 primary antibody (3 μg/ml, R&D Systems Ltd.). After three washes with PBS and incubation with secondary antibody linked to horseradish peroxidase (DAKO; Glostrup, Denmark) for 1 h at room temperature, DAB staining was performed using a DAB peroxidase substrate kit. Nuclei were counterstained with hematoxylin, and the sections were dehydrated in a series of ethanol and xylene before application of coverslips. Negative controls were processed in the same manner without the primary antibody. Semi-quantitative immunohistochemical analysis of Gr-1 positive staining in liver tissue was conducted.

Determination of oxidative stress

Oxidative stress after 24 h of reperfusion was assessed via evaluation of the lipid peroxidation marker, 4-hydroxynonenal (HNE), and reactive oxygen species (ROS) generating NADPH NOX2. HNE in hepatic tissues was determined using a specific kit (Cell Biolabs, San Diego, CA, U.S.A.). In brief, BSA or hepatic tissue extracts (10 mg ml^{-1}) were adsorbed onto a 96-well plate for 12 h at 4°C. HNE adducts present in the sample or standard were probed with an anti-HNE antibody, followed by an HRP-conjugated secondary antibody. HNE–protein adducts in experimental samples were assessed based on a standard curve. NOX2 activity was measured using the cytochrome *c* reduction assay. Briefly, 100 μg liver tissue proteins from different groups were incubated in 25 mM HEPES buffer (pH 7.0) with 150 μm cytochrome *c* and 100 μm NADPH for 30 min at 37°C. Cytochrome *c* reduction was measured by determining absorbance at 550 nm. For further confirmation, ROS production in non-parenchymal cells from livers in different groups was detected using confocal imaging with a Zeiss LSM510 and LSM710 system (Carl Zeiss AG) after loading with 5-chloromethyl-2,7-dichlorodihydrofluorescein diacetate acetyl ester (DCFH-DA, 4.5 M; excitation, 488 nm; emission, 505–550 nm). In light of the saturation of the probe monitoring obtained, quantitative analyses were further performed via flow cytometric detection (BD Biosciences) following treatment of cells with DCFH-DA for 30 min.

Analysis of neutrophil-LSEC adhesion

LSECs were grown to confluence in six-well confocal plates and treated with tryptase for 24 h. Primary neutrophils labeled with CFSE were added to each well under the same conditions for 1 h. After incubation, the neutrophil-containing medium was aspirated and the monolayer gently washed three times with PBS to remove the unbound neutrophils. Fluorescence was measured at excitation and emission wavelength of 488 and 535 nm, respectively, using a Leica DMI6000 fluorescence microscope (Leica, Germany), and the number of adherent cells was analyzed using ImageJ (NIH). Individual treatments were performed in duplicate, and the entire set of experiments was repeated three times.

Statistical analysis

Results are expressed as the mean values ± SEM. The differences among experimental groups were evaluated using Student's *t*-tests or ANOVA where appropriate, and significance of differences between groups was assessed via Newman–Keuls post-hoc test. Analysis was performed using a statistical software package (GraphPad-Prism 7; GraphPad, La Jolla, CA, U.S.A.) and significance defined as $P<0.05$.

Results

Hepatic I/R-induced injury is associated with pathological alterations in gastrointestinal tissue

We analyzed alterations in time-course of liver pathology and hepatocellular function in wild-type C57BL/6 mouse livers subjected to 60 min warm ischemia followed by 1, 3, 6, 12, and 24 h reperfusion (Figure 1A). The levels of ALT and AST enzymes, markers of hepatocellular damage, were assessed in sera of wild-type C57BL/6 mice during I/R. Compared with sham controls, both serum ALT and AST levels were increased in different hepatic I/R groups, particularly after 6 h reperfusion (2174.8 ± 318.9 U/l). And all observed changes in different groups were pooled in Figure 1B. These data correlated with *Suzuki's* histological grading of liver I/R damage (Figure 1C,D). Mouse

© 2018 The Author(s). This is an open access article published by Portland Press Limited on behalf of the Biochemical Society and distributed under the Creative Commons Attribution License 4.0 (CC BY-NC-ND).

Clinical Science (2018) **132** 2241–2259
https://doi.org/10.1042/CS20180662

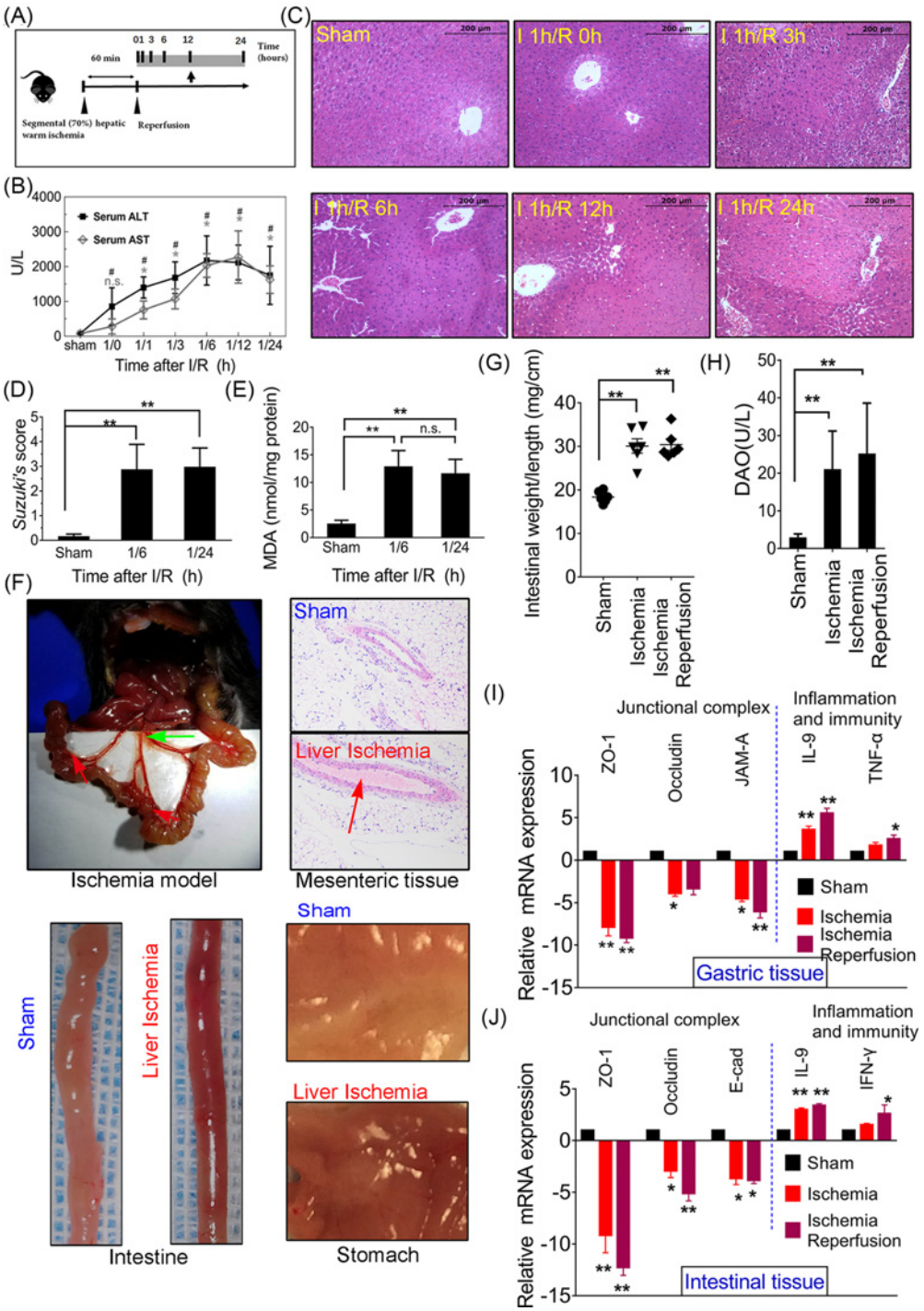

Figure 1. Hepatic I/R-induced injury is associated with pathological alterations in gastrointestinal tissue

(**A**) Flow chart of mouse liver I/R model establishment. (**B**) Liver damage/necrosis markers, ALT and AST, are significantly elevated in mouse serum upon I/R induction at 1, 3, 6, 12, and 24 h after reperfusion. (**C**) Liver histology (H&E staining) of mice subjected to sham surgery or 1 h ischemia followed by 0, 3, 6, 12, and 24 h of reperfusion showing representative images of coagulation necrosis (lighter areas). (**D** and **E**) Comparison of the *Suzuki's* score of liver damage and MDA levels between different time-points. (**F**) Tissue congestion in both intestine and stomach under 60 min of warm liver ischemia compared with sham controls. (**G**) Intestinal weight/length and (**H**) the level of DAO are significantly increased under liver I/R conditions. RT-PCR analysis of key junctional complex regulatory genes, MCs related pathological immune gene, and inflammatory gene in (**I**) stomach and (**J**) intestine following liver ischemia or ischemia reperfusion. Data are presented as mean ± SEM; n=3–10 mice/group. n.s., not significant, $^{*}P<0.05$ and $^{**}P<0.01$ in comparisons between I/R and sham groups, and $^{\#}P<0.05$ for serum ALT data comparisons.

© 2018 The Author(s). This is an open access article published by Portland Press Limited on behalf of the Biochemical Society and distributed under the Creative Commons Attribution License 4.0 (CC BY-NC-ND).

models of hepatic I/R displayed sinusoidal congestion and similar findings were recorded in livers subjected to 60 min of warm ischemia. In addition, livers displayed multiple vacuolization, moderate to severe edema, and extensive tissue necrosis at 6, 12, and 24 h reperfusion compared with sham controls (Figure 1C,D; *Suzuki's* score: 2.88 ± 0.41, 3.02 ± 0.42 and 2.98 ± 0.37 vs 0.28 ± 0.14, respectively; $P<0.01$). Liver H&E staining revealed no necrotic areas in the sham control group. Considering that oxidative damage is critical in the hepatic I/R process, MDA activity (nmol/mg protein) was used as an index to assess liver oxidative status in tissue homogenates. Notably, MDA levels were significantly increased after 6 and 24 h of reperfusion (Figure 1E; 12.93 ± 1.16 and 11.67 ± 1.02 vs 2.53 ± 0.25; $P<0.01$).

Analogous to clinical portal hypertensive patients with splenomegaly and gastrointestinal bleeding, a hepatic I/R model constructed with blockage of blood flow into the mouse liver should inevitably lead to gastrointestinal congestion. Pathological changes of congestion in intestine (red arrow) and mesenteric vessels (green arrow) were observed in the model of liver ischemia, which are consistent with the H&E results that blood cells are deposited in microvasculature of mesenteric tissue (red arrow). Histological examination of intestine and stomach revealed evident congestion following 60 min of warm liver ischemia (Figure 1F). In addition, the ratio of intestinal weight/length was increased in the context of ischemia and ischemia/reperfusion (Figure 1G, $P<0.01$). Up-regulation of serum diamine oxidase (DAO) activity (U/l) usually occurs during impairment of gastrointestinal mucosal barrier function. Consistent with this finding, we detected a significant increase in serum DAO in the mouse hepatic I/R model compared with sham controls (Figure 1H; 21.08 ± 4.13 and 25.23 ± 5.46 vs 2.98 ± 0.37, respectively; $P<0.01$). We next examined the cell–cell junctional complex, the essential structural component of the epithelial barrier, and immune cytokines related to the tissue environment of stomach and intestine. The mRNA levels of these key junctional-complex markers were markedly diminished, while the levels of IL-9, TNF-α, and IFN-γ cytokines increased in the I/R model (Figure 1I, J; $P<0.01$ or $P<0.05$). The collective results implied a close relationship between liver damage and gastrointestinal pathological changes during the hepatic I/R process.

Activation of gastrointestinal MCs mediates liver injury during hepatic I/R

The MC numbers and activation status differs among various organs. As MCs specifically and highly express tryptase, chymase, CD117(c-Kit), and the receptor for IgE, FcεRI, we used a combination of these markers to confirm that MCs predominantly localize in the gastrointestinal tract. Levels of both c-Kit and tryptase were higher in gastrointestinal tissue than other regions of normal wild-type C57BL/6 mice (Figure 2A). In addition, immunohistochemistry for tryptase and flow cytometry for detecting c-Kit+ FcεRI+ gated on CD45+ CD11b- among mononuclear cells disclosed considerable amounts of MCs in the stomach and intestine. However, we observed almost no MCs in the liver (Figures 2B,C; tryptase + cells/HPF in liver: 0.20 ± 0.13, intestine: 4.7 ± 1.61, stomach: 10.4 ± 2.8; Kit+ FcεRI+ cells in the liver: 0.27 ± 0.08%, intestine: 5.30 ± 0.80%, stomach: 12.8 ± 1.26%).

Analysis of toluidine blue staining further confirmed the lack of MCs in liver tissue relative to stomach, intestine, and mesentery. Furthermore, the number of liver MCs did not change even during hepatic I/R (Figure 2D). Tryptase and histamine production is generally used as indicators of MC degranulation and represents the main mediators secreted by MCs in direct contact with liver tissue through blood circulation; that are potentially involved in pathogenesis of hepatic I/R, tryptase, and histamine secretion by MCs in both sham and I/R groups was examined. In Figure 2E,F, increased production of both histamine (nM) and MCP-7 trypase of TPSAB1 (ng/ml) by MCs after I/R induction relative to sham surgery is shown. These trends are similarly time dependent. In fact, MC degranulation had already occurred at the ischemia stage and reached a peak after 3 h of reperfusion (serum histamine level: 75.51 ± 5.59; serum tryptase level: 2.886 ± 0.322). To further ascertain the effect of gastrointestinal MC degranulation on liver injury during hepatic I/R, we analyzed the correlations between degranulation factors and liver injury. MCs are filled with dense particles (solid arrow) ready to respond to the attack from different pathogens. In I/R mice, MC degranulation (hollow arrow and red circle) was evident in both stomach and intestine, consistent with the increased level of histamine and tryptase. Our data further showed significant positive correlations between the percentage of degranulated gastrointestinal MCs and *Suzuki's* score, level of ALT, and MDA activity (Figure 2G, $P<0.05$ or $P<0.01$). Based on these findings, we speculate that gastrointestinal MCs are inevitably activated during the hepatic I/R process, and their subsequent degranulation releases components that are transported to the liver blood supply system and contributing, at least in part, to liver damage.

Significant reduction of hepatic I/R injury in MC-deficient mice

To determine the specific role of gastrointestinal MCs in hepatic I/R injury, the extent of liver injury was analyzed in groups of c-Kit mutant MC-deficient (Kit $^{W\text{-}sh/W\text{-}sh}$) mice and compared with that in wild-type or Kit $^{W\text{-}sh/W\text{-}sh}$ RMC

© 2018 The Author(s). This is an open access article published by Portland Press Limited on behalf of the Biochemical Society and distributed under the Creative Commons Attribution License 4.0 (CC BY-NC-ND).

Clinical Science (2018) **132** 2241–2259
https://doi.org/10.1042/CS20180662

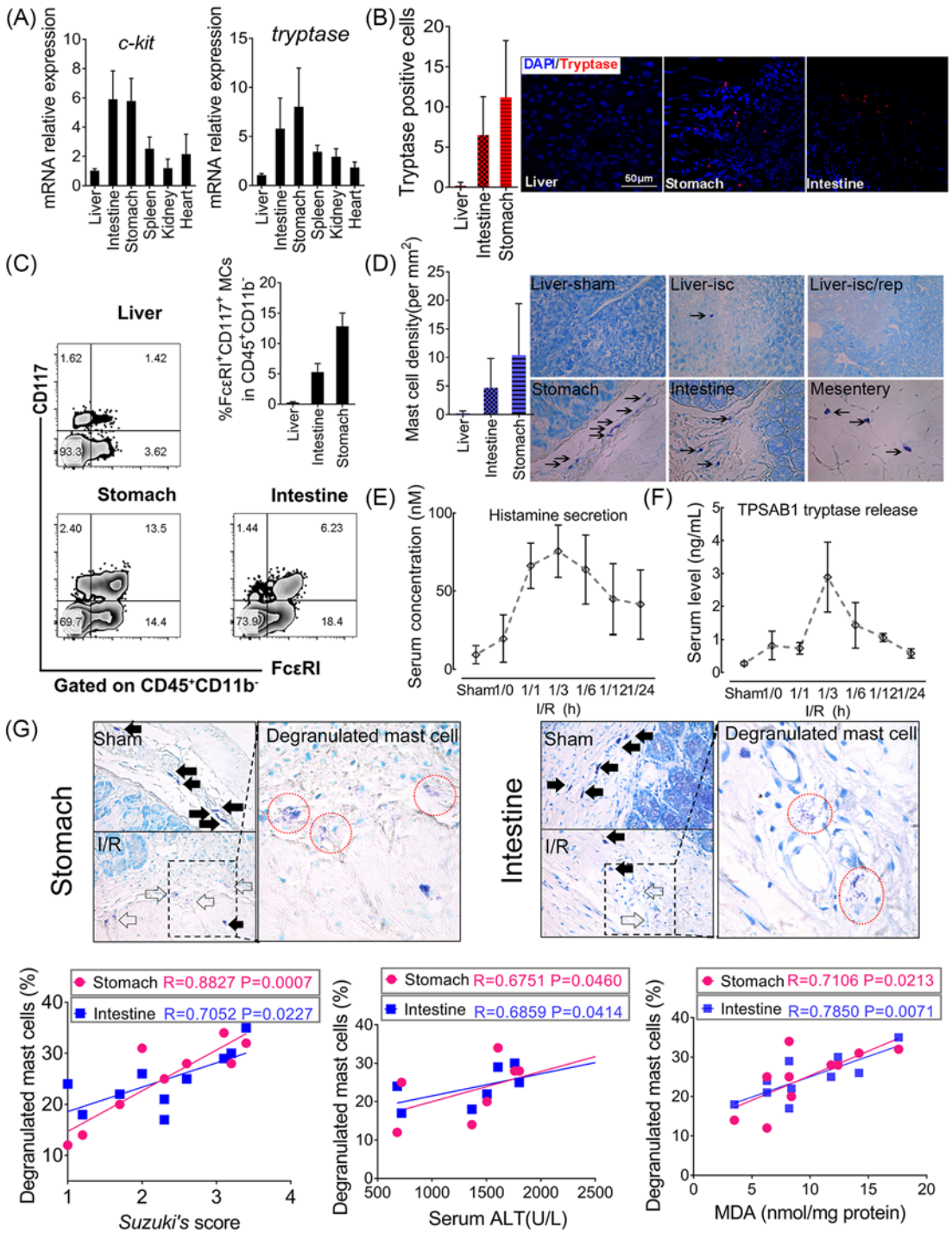

Figure 2. Degranulation of mast cells, tissue-resident immune cells abundant in the gastrointestinal system, is significantly associated with liver damage during the hepatic I/R process

(**A**) Application of RT-PCR to determine the expression of MC-specific markers (c-Kit & Tryptase) in normal organs. (**B**) Immunofluorescence of tryptase-positive cells (MCs) in liver, stomach, and intestine. (**C**) FACS analysis of CD117+FceRI+ cells (MCs) gated on CD45+CD11b- in liver, stomach, and intestine. (**D**) Toluidine blue staining to determine MC density in tissues of liver, stomach, intestine, and mesentery. (**E** and **F**) Serum histamine and tryptase levels during liver I/R injury. (**G**) Representative toluidine blue stain of gastrointestinal section shows the degranulated MCs in liver I/R process. Percentages of degranulated MCs in the stomach and intestine are positively correlated with *Suzuki's* score for liver damage, serum ALT (U/l), and MDA (nmol/mg protein) levels. Data are presented as mean ± SEM, n=3–5 mice/group for (A), (B), and (C); n=10 mice/group for (E) and (F).

© 2018 The Author(s). This is an open access article published by Portland Press Limited on behalf of the Biochemical Society and distributed under the Creative Commons Attribution License 4.0 (CC BY-NC-ND).

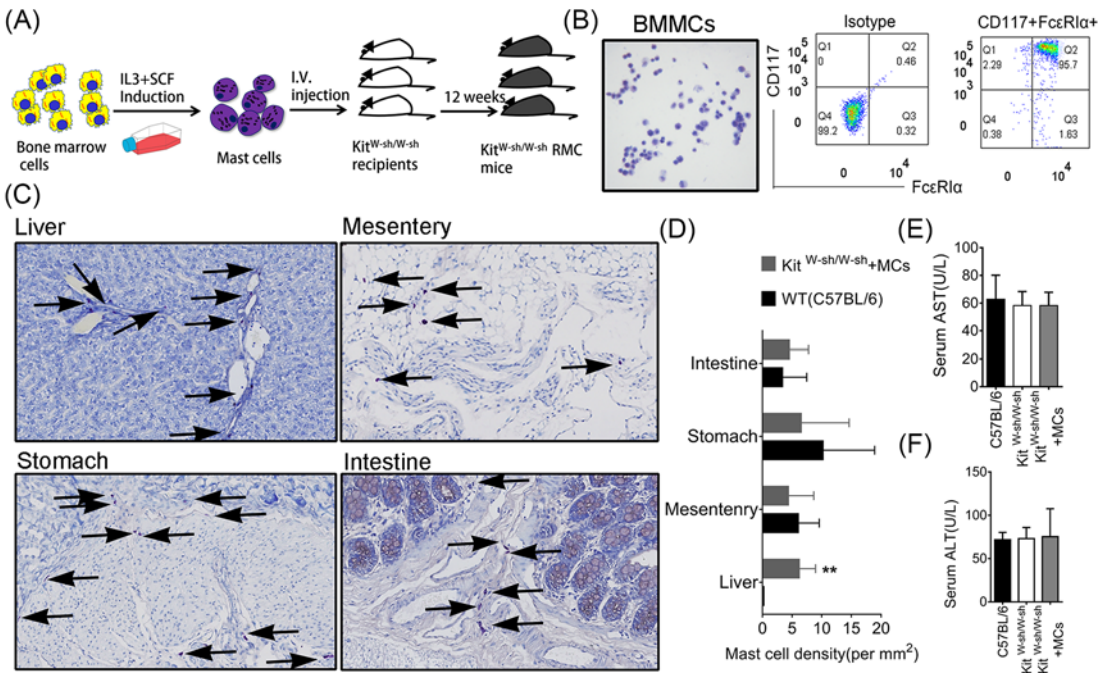

Figure 3. Engraftment of MC-deficient mice with BMMCs

(**A**) Flowchart of reconstitution of Kit $^{W\text{-}sh/W\text{-}sh}$ mice with BMMCs. (**B**) The representative images of BMMCs stained with toluidine blue and flow cytometric evaluation of the purity of BMMC preparation. (**C** and **D**) Analysis of the distribution and number of MCs in liver, mesentery, stomach, and intestine after MC engraftment into Kit $^{W\text{-}sh/W\text{-}sh}$ mice using a high-throughput digital pathology section scanner. MCs are indicated with arrows. Under normal condition, there is no significant difference in serum levels of (**E**) AST and (**F**) ALT between C57BL/6, Kit $^{W\text{-}sh/W\text{-}sh}$, and Kit $^{W\text{-}sh/W\text{-}sh}$ + MCs mice. Data are presented as mean ± SEM, n=8 mice/group for Kit $^{W\text{-}sh/W\text{-}sh}$ + MCs group and Kit $^{W\text{-}sh/W\text{-}sh}$ group; n=6 for C57BL/6 mice. $^{**}P<0.01$ in comparisons between Kit $^{W\text{-}sh/W\text{-}sh}$ + MCs and C57BL/6 mice.

mice. To generate Kit $^{W\text{-}sh/W\text{-}sh}$ RMC mice, highly pure MCs were obtained from differentiated bone marrow cells and transferred into Kit $^{W\text{-}sh/W\text{-}sh}$ mice via intravenous (i.v.) injection (Figure 3A). Bone marrow cells were obtained from congenic mice with phagocytosis in toluidine blue-stained sections following differentiation into MCs after 5 weeks of culture. The purity of MCs, evaluated as a percentage of c-Kit+ and FcεRIα+ cells, was >95% (Figure 3B). Transmission electron microscopy was employed to detect the phenomenon of MC degranulation (data not shown). After 12 weeks of MC infusion, successful generation of Kit $^{W\text{-}sh/W\text{-}sh}$ RMC mice was confirmed. A significant number of MCs were found in the liver of Kit $^{W\text{-}sh/W\text{-}sh}$ RMC mice ($P<0.01$), and the MC density in stomach, intestine, and mesentery was similar to that in the wild-type mice (Figure 3C,D). The normal control among wild-type and MC-deficient Kit $^{W\text{-}sh/W\text{-}sh}$ and Kit $^{W\text{-}sh/W\text{-}sh}$ RMC mice did not show liver injury, and similar results were obtained in the level of serum AST (Figure 3E, no significant difference) and ALT (Figure 3F, no significant difference).

Next, we examined pathological alterations under hepatic I/R injury conditions. Large necrotic areas were observed in liver lobes of Kit $^{W\text{-}sh/W\text{-}sh}$ RMC mice following 60 min of ischemia both 6 and 24 h of reperfusion, whereas the extent of necrotic areas and *Suzuki's* score in MC-deficient mice were remarkably reduced compared with wild-type C57bl/6 and Kit $^{W\text{-}sh/W\text{-}sh}$ RMC mice (Figure 4A). MC deficiency resulted in minimal vacuolization, edema, and necrosis following reperfusion for 6 and 24 h, respectively (Figure 4B; scores, 2.55 ± 0.22 and 2.99 ± 0.15, respectively). In contrast, livers of wild-type or Kit $^{W\text{-}sh/W\text{-}sh}$ mice reconstituted with MCs displayed moderate to severe edema and extensive hepatocellular necrosis (Figure 4B; scores of C57BL/6 mice: 3.23 ± 0.18 and 3.43 ± 0.19, scores of Kit $^{W\text{-}sh/W\text{-}sh}$ RMC mice: 3.36 ± 0.27 and 3.27 ± 0.25, respectively, $P<0.01$). Serum ALT and AST levels in Kit $^{W\text{-}sh/W\text{-}sh}$ mice were significantly decreased ($P<0.01$ or $P<0.05$), compared with wild-type C57BL/6 and Kit $^{W\text{-}sh/W\text{-}sh}$ RMC mice following 6 and 24 h reperfusion (Figure 4C,D). Consistent with liver injury observed from both histological and biochemical evaluations (based on serum ALT/AST levels), our results disclosed cellular apoptosis under conditions of hepatic I/R damage following 24 h of reperfusion (data from sham groups are not shown). Moreover, depletion of MCs led to significantly reduced liver cell apoptosis based on semi-quantitative evaluation of TUNEL staining (Figure

© 2018 The Author(s). This is an open access article published by Portland Press Limited on behalf of the Biochemical Society and distributed under the Creative Commons Attribution License 4.0 (CC BY-NC-ND).

Clinical Science (2018) **132** 2241–2259
https://doi.org/10.1042/CS20180662

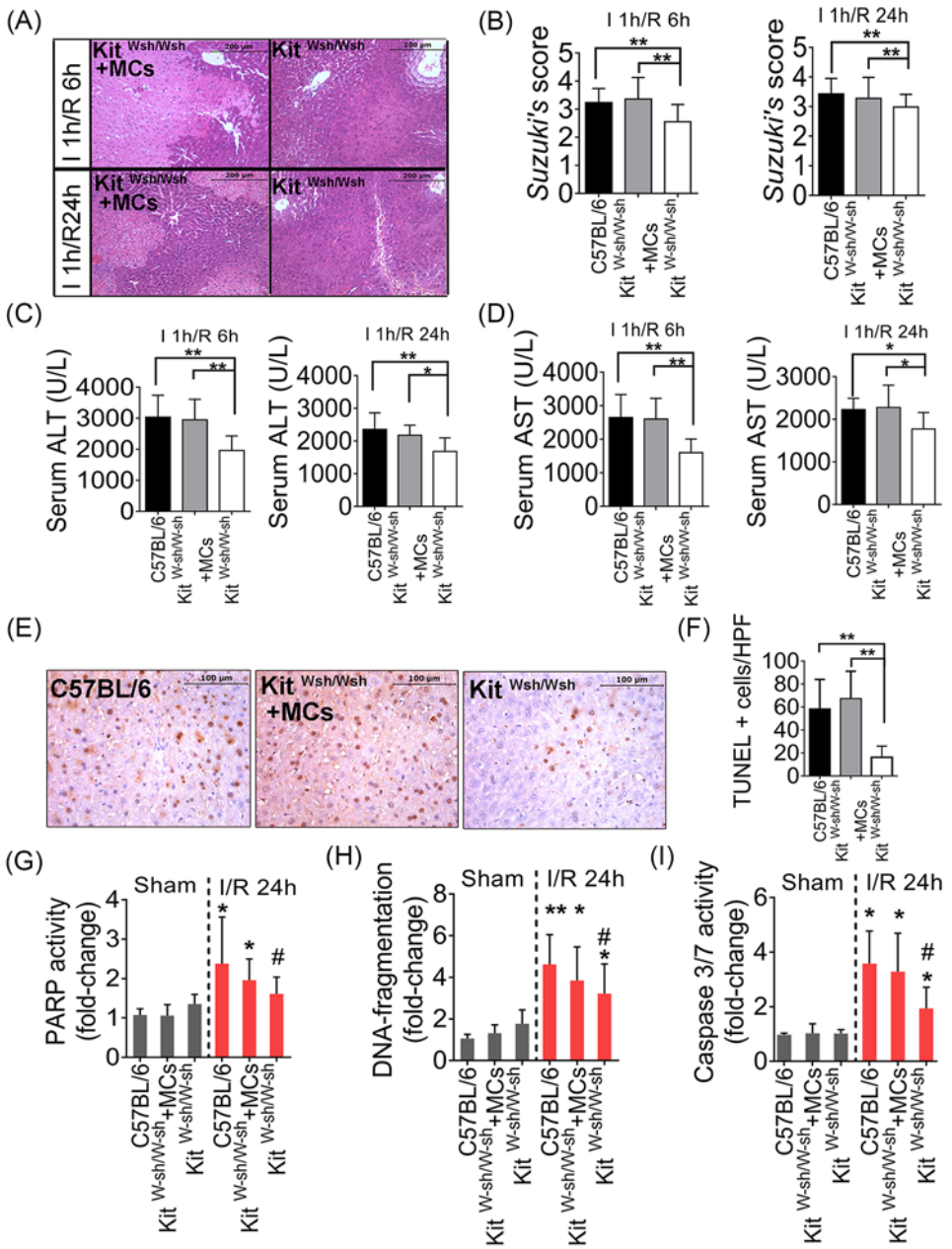

Figure 4. Hepatic I/R injury is significantly reduced in Kit$^{W\text{-}sh/W\text{-}sh}$ MC- deficient compared with wild-type and Kit $^{W\text{-}sh/W\text{-}sh}$ RMC mice

(**A** and **B**) Representative H&E-stained sections of liver from Kit $^{W\text{-}sh/W\text{-}sh}$ and Kit $^{W\text{-}sh/W\text{-}sh}$ RMC mice, and the corresponding *Suzuki's* scores were counted and compared at 6 or 24 h after reperfusion. (**C** and **D**) Serum ALT and AST levels. (**E** and **F**) Representative TUNEL staining in liver tissue showing the number of cells in wild-type C57BL/6, Kit $^{W\text{-}sh/W\text{-}sh}$, and Kit $^{W\text{-}sh/W\text{-}sh}$ RMC mice undergoing apoptotic death at 6 or 24 h after reperfusion. (**G**, **H**, and **I**) Comparison of cell death markers (caspase 3/7 activity, DNA fragmentation, and PARP activity). Data are presented as mean ± SEM, n=6–10 mice/group; $^{*}P<0.05$ and $^{**}P<0.01$ for comparisons among wild-type C57BL/6, Kit $^{W\text{-}sh/W\text{-}sh}$, and Kit $^{W\text{-}sh/W\text{-}sh}$ RMC mice in (A), (B), and (C). $^{*}P<0.05$ and $^{**}P<0.01$ between I/R and sham groups, $^{\#}P<0.05$ among wild-type, C57BL/6, Kit $^{W\text{-}sh/W\text{-}sh}$, and Kit $^{W\text{-}sh/W\text{-}sh}$ RMC mice (G, H, and I).

© 2018 The Author(s). This is an open access article published by Portland Press Limited on behalf of the Biochemical Society and distributed under the Creative Commons Attribution License 4.0 (CC BY-NC-ND).

4E,F; 58.41 ± 10.20/72.25 ± 8.21 vs 16.25 ± 3.43, respectively, $P<0.01$). Both necrotic (PARP activity) and apoptotic cell death markers (caspase 3/7 activity and DNA fragmentation) in liver were additionally evaluated. Levels of all cell death markers in liver were markedly increased at 24 h of reperfusion following 60 min of ischemia. Kit $^{W\text{-}sh/W\text{-}sh}$ mice with MC deficiency showing significantly attenuated marker levels, compared with the other groups (Figure 4G,H, and I; $P<0.01$ or $P<0.05$). Thus, liver injury following I/R is markedly reduced in the absence of MCs, as assessed based on histology, blood chemistry, and cell death markers.

Degranulation of gastrointestinal MCs induces LSEC death following hepatic I/R injury

LSECs line hepatocytes across the perisinusoidal space (or space of *Disse*) play a significant role in transport of nutrients and biological mediators from circulating blood to the liver. Under conditions of liver I/R in wild-type C57BL/6 mouse, H&E staining revealed the swelling, lining, and embolization of microvascular (red arrow) after 3 h reperfusion. Compared with sham mice, the endothelial cell damage (blue arrow) and blocked sinusoidal blood flow were observed followed 6 and 24 h reperfusion, respectively (Figure 5A,B). Degranulation mediators of gastrointestinal MCs reach liver tissue via the blood circulation and initially interact with LSECs to regulate their pathological development in response to hepatic I/R. As expected, our results indicate that absence of MCs was beneficial for LSEC survival during hepatic I/R (Figure 5C; 28.86 ± 3.22 vs 39.85 ± 5.40, $P<0.05$). VCAM-1 and ICAM-1 typically expressed on endothelial cells are known for their importance in stabilizing cell–cell interactions and facilitating leukocyte endothelial transmigration. The levels of these adhesion molecules were significantly elevated in response to LSEC damage compared with sham controls. Our data further supported impairment of signaling of both ICAM-1 and VCAM-1 in the absence of gastrointestinal MCs during hepatic I/R injury (Figure 5D; ICAM-1: 81.37 ± 17.27 vs 52.48 ± 10.59; Figure 5E; VCAM-1: 96.53 ± 13.67 vs 64.58 ± 12.81, respectively, $P<0.05$). Thrombosis in liver microcirculation is closely related to LSEC damage during I/R. The higher TxB2:6-keto-PgF1α ratio in I/R model compared with that in sham significantly reflects thrombosis induced by LSEC damage (Figure 5F; Kit $^{W\text{-}sh/W\text{-}sh}$: 0.28 ± 0.04 vs 0.52 ± 0.07, C57BL/6: 0.25 ± 0.03 vs 0.68 ± 0.11, $P<0.05$). In keeping with above results, we observed a significant lower TxB2/6-keto-PgF1α ratio in Kit $^{W\text{-}sh/W\text{-}sh}$ mice subjected to I/R compared with wild-type mice ($P<0.05$).

To further confirm the effect of MC degranulation to LSECs, we isolated LSECs from the mouse liver via a negative selection method using CD11b-MACS combined with long-term selective adherence. Purity of the final cell preparation reached more than 95%. Analysis under a scanning electron microscope revealed typical LSEC fenestrations organized in sieve plates (Figure 5G). Given that polyfunctional tryptase is the main granule compound of MCs and used to define the subset of MCs located mainly around blood vessels, ICAM-1 and VCAM-1 expression were further analyzed on LSECs treated with tryptase or MC granule containing media. Consistent with *in vivo* findings, both ICAM-1 and VCAM-1 expression were enhanced following MC degranulation or the tryptase (Figure 5H,I,J; ICAM: tryptase: 41.73 ± 1.53%, MC granulation: 46.13 ± 1.16% vs control: 13.80 ± 1.36%, $P<0.01$; VCAM: tryptase: 23.87 ± 0.77%, MC granulation: 34.53 ± 3.47% vs control: 5.59 ± 0.95%, $P<0.01$).

Degranulation of gastrointestinal MCs enhances neutrophil liver infiltration and NET formation during experimental I/R injury

Studies on hepatic I/R injury have revealed an acute inflammatory response characterized by increased adhesion and aggregation of neutrophils in the sinusoids and emigration of immune cells into parenchyma. Considering the possible association between gastrointestinal MC activation after hepatic I/R injury and inflammatory cell infiltration, we further investigated whether MC degranulation regulates neutrophil filtration, NET formation, and signaling of the neutrophil-specific enzyme MPO. Using a specific marker for neutrophils, we demonstrated significant reduction in infiltration of liver neutrophils in MC-depleted mice, compared with their C57BL/6 counterparts at 24 h post-I/R (Figure 6A,B; CD45+Ly6G+CD11b+neutrophils: 10.50 ± 1.95% vs 15.28 ± 2.38%, Gr-1+neutrophils: 46.00 ± 8.62 vs 85.33 ± 20.47, respectively, $P<0.05$) and limited neutrophil infiltration in sham controls (data on Gr-1+ neutrophils in the sham group are not shown). In addition, activity of MPO, a neutrophil-specific enzyme, was significantly increased in the liver 24 h after I/R. As expected, we detected a significant reduction in MPO activity after MC depletion (Figure 6C; 3.70 ± 0.88 vs 5.33 ± 1.06, $P<0.05$). To determine whether infiltrated neutrophils form NETs after injury, we initially measured NET formation in sera of mice undergoing liver I/R. When neutrophils form NETs, chromatin DNA associated with other neutrophil proteins is released locally and then distributed in the circulation. The quantity of NET–DNA complexes was dramatically elevated in mice experiencing I/R (Figure 6D,E). Furthermore, I/R liver lobes contained citrullinated-histone H3. Importantly, NET formation was significantly inhibited in mice without

© 2018 The Author(s). This is an open access article published by Portland Press Limited on behalf of the Biochemical Society and distributed under the Creative Commons Attribution License 4.0 (CC BY-NC-ND).

Clinical Science (2018) **132** 2241–2259
https://doi.org/10.1042/CS20180662

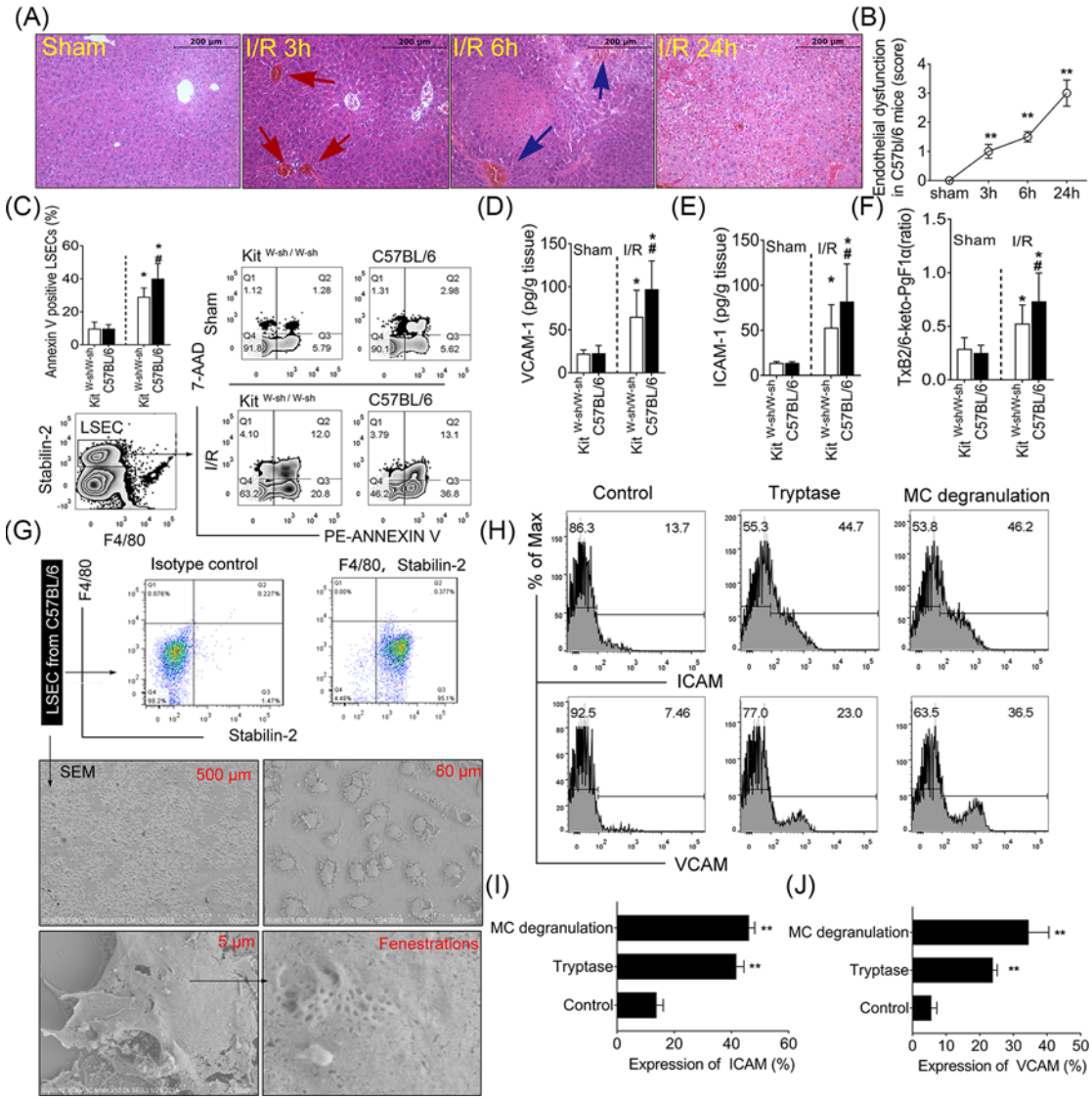

Figure 5. Degranulation of gastrointestinal MCs induces LSEC death following hepatic I/R injury

(**A**) Representative H&E stained sections of liver show the vascular pathological changes during I/R. (**B**) Evaluation of endothelial dysfunction. (**C**) Flow cytometry analysis to determine Annexin V-positive LSECs. (**D** and **E**) Expression of adhesion molecules (VCAM-1 and ICAM-1) in liver tissue. (**F**) Ratio of TxB2 to 6-keto-PgF1α. (**G**) Representative flow cytometry plots and scanning electron microscopy show the purity and typical fenestrations characteristic of isolated LSECs, respectively. (**H**, **I**, and **J**) Representative plots and mean percentage of ICAM and VCAM for isolated LSECs in control, tryptase treatment, and MC granule treatment. Data are presented as mean $\pm$ SEM, n=6–10 mice/group; $^{**}P<0.01$ in comparisons between different time points in (B). $^{*}P<0.05$ and $^{**}P<0.01$ in comparisons between I/R and sham groups, $^{\#}P<0.05$ between wild-type C57BL/6 and Kit $^{W\text{-}sh/W\text{-}sh}$ mice in (D), (E), and (F). $^{**}P<0.01$ for comparing with control in (I and J), and data were pooled from three repeated experiments.

MCs (NET–DNA: 5.625 $\pm$ 0.751 vs 8.987 $\pm$ 1.532; Cit-H3: 1.058 $\pm$ 0.178 vs 1.323 $\pm$ 0.205). The collective data supported a stimulatory role of early MC activation in the gastrointestinal system in the inflammatory response during liver I/R through promoting pathological neutrophil recruitment and NET formation.

Degranulation of gastrointestinal MCs initiates a cytokine cascade and increase in oxidative stress in experimental hepatic I/R

Here, we examined local inflammatory responses in liver tissue via quantitative RT-PCR analysis of chemokine/cytokine mRNA levels in liver extracts. MC deletion was associated with selective reduction in the

© 2018 The Author(s). This is an open access article published by Portland Press Limited on behalf of the Biochemical Society and distributed under the Creative Commons Attribution License 4.0 (CC BY-NC-ND).

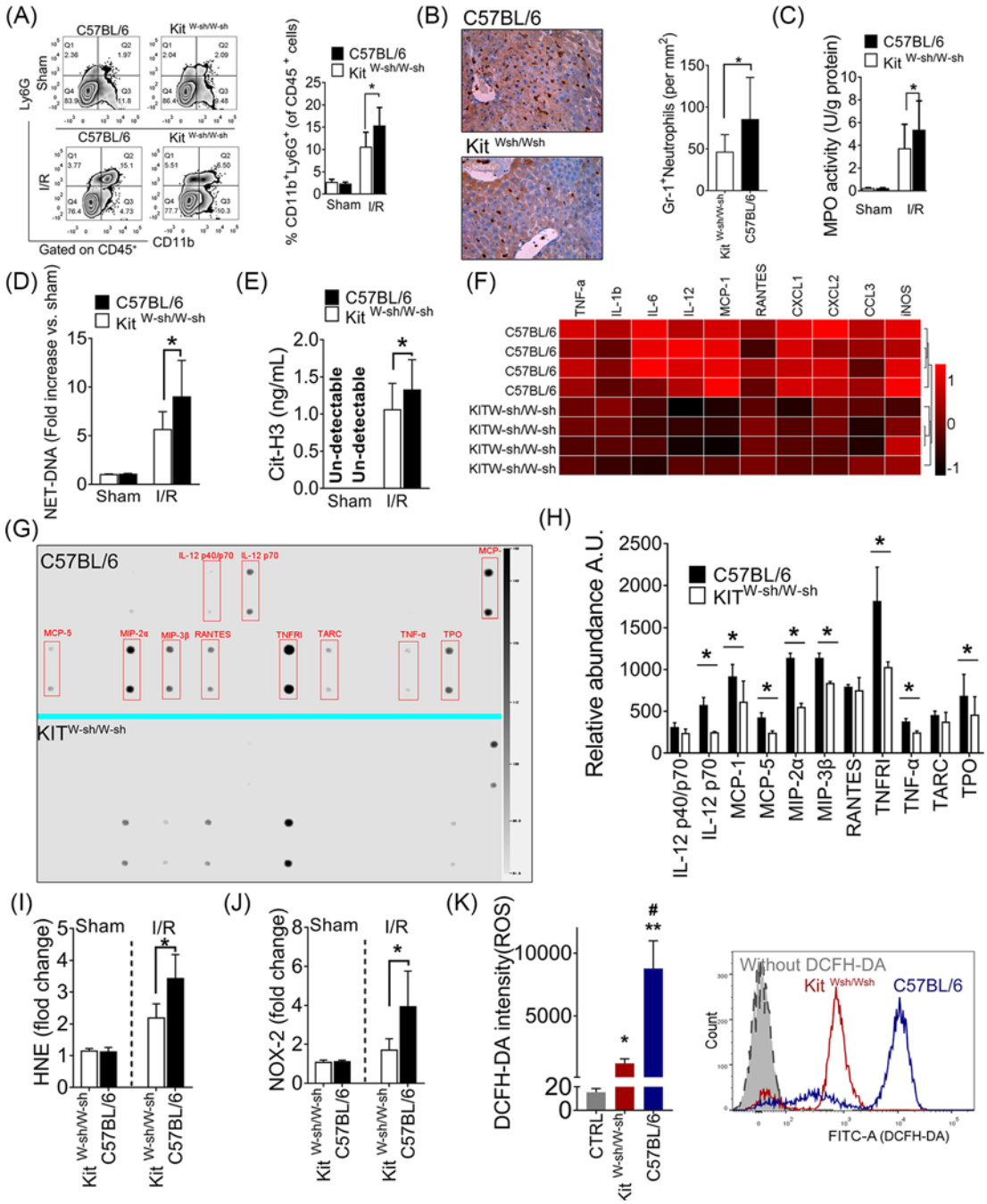

Figure 6. Degranulation of gastrointestinal MCs enhances neutrophil liver infiltration and NET formation, and triggers a cytokine cascade and oxidative stress during experimental I/R injury

(**A**) FACS analysis to determine the CD11b+Ly6G+ neutrophil population from CD45+ cells. (**B**) IHC to determine Gr-1+ neutrophil infiltration with liver sections. (**C**) Neutrophil sequestration within the liver was quantified by measuring tissue MPO activity. (**D**) NET–DNA complexes and (**E**) levels of CitH3 for determining NET formation. (**F**) Quantitative RT-PCR assessment of chemokine/cytokine mRNA levels in liver extracts. (**G** and **H**) Analysis of chemokine/cytokine expressions with the RayBiotch antibody array. (**I** and **J**) Assessment of late oxidative stress markers, HNE and NOX-2, after 24 h of reperfusion (I/R 24 h). (**K**) Analysis of ROS production of non-parenchymal cells in liver via DCFH-DA intensity detected with FACS. Data are presented as mean ± SEM, n=6 10 mice/group; $^{*}P<0.05$ and $^{**}P<0.01$ in comparisons between wild-type C57BL/6 and Kit $^{W\text{-}sh/W\text{-}sh}$ mice in (A–J). $^{*}P<0.05$ and $^{**}P<0.01$ for comparing with control, and $^{\#}P<0.05$ between wild-type C57BL/6 and Kit $^{W\text{-}sh/W\text{-}sh}$ mice in (K).

© 2018 The Author(s). This is an open access article published by Portland Press Limited on behalf of the Biochemical Society and distributed under the Creative Commons Attribution License 4.0 (CC BY-NC-ND).

Clinical Science (2018) **132** 2241–2259
https://doi.org/10.1042/CS20180662

expression of several proinflammatory cytokines/chemokines classically up-regulated within 24 h after I/R injury, including TNF-α, IL-6, IL-12, MCP-1, CXCL2, and iNOS (Figure 6F; $P<0.05$ or $P<0.01$). Semi-quantitative results of antibody arrays further showed that MC deficiency lead to a significant decrease in the expression of a set of proinflammatory cytokines/chemokines (Figure 6G,H), which play critical roles in promoting liver I/R injury ($P<0.05$).

Oxidant attack is critically involved in organ damage after liver I/R. Delayed oxidative stress induced by liver I/R, measured based on expression of the lipid peroxidation marker, 4-hydroxynonenal (HNE), and the reactive oxygen species (ROS) generating NADPH oxidase isoform 2 (NOX2), was reduced in Kit $^{W\text{-}sh/W\text{-}sh}$ mice (Figure 6I,J; $P<0.05$). Furthermore, MC deficiency induced a decrease in ROS of non-parenchymal cells in livers subjected to I/R injury (Figure 6K; DCFH-DA intensity in the control group: 15.47 ± 1.82, Kit $^{W\text{-}sh/W\text{-}sh}$: 1218.00 ± 203.42, C57BL/6 :8772.67 ± 1277.76; $P<0.05$ or $P<0.01$). These findings were consistent with both histological and biochemical observations.

The granule component of MCs is involved in LSEC-related inflammation *in vitro*

Endothelial–neutrophil interactions are essential for regulation of the inflammatory response in liver I/R. To further confirm whether MC degranulation exerted a direct effect on LSEC function, we isolated neutrophils from mice and evaluated the effect of tryptase on adhesion of neutrophils to LSECs. As shown in Figure 7A, 1 ng/ml tryptase treatment of LSECs for 24 h was able to sufficiently increase neutrophil adhesion as compared with control group, suggesting that the tryptase efficiently triggered and promoted neutrophil infiltration (1 ng/ml: 176.0 ± 23.77, 10 ng/ml 168.5 ± 22.9, 100 ng/ml 219.3 ± 36.7 vs control: 92.5 ± 21.4, $P< 0.05$ or $P< 0.01$). In view of the complexity of *in vivo* conditions in a liver I/R animal model, the system of non-parenchymal cells (NPCs) in livers was additionally employed to assess the role of MC degranulation *in vitro*. Consistent with *in vivo* findings, treatment with tryptase or MC granule component led to a significant increase in TNF-α, MCP-1, and ROS content relative to the control group (Figure 7B–D; TNF-α: tryptase: 52.88 ± 14.90, MC degranulation: 101.70 ± 17.13 vs control: 8.10 ± 2.67; MCP-1: tryptase: 18.33 ± 3.03, MC degranulation: 17.85 ± 1.95 vs control: 11.03 ± 4.79; relative ROS content: tryptase: 3127 ± 164, MC degranulation: 6485 ± 1095 vs control: 2014 ± 363; $P<0.05$ or $P<0.01$).

Discussion

To our knowledge, the present study is the first to focus on the role of gastrointestinal MCs in hepatic I/R injury contacting at a distance via the liver blood supply system. We observed that MCs predominantly localized in mouse gastrointestinal and mesentery tissue but were practically absent in liver, consistent with previous findings [17]. Interestingly, gastrointestinal MCs were activated during liver I/R injury. While the mechanisms underlying MC activation remain to be established, gastrointestinal MC degranulation is proposed to exert a deleterious effect on liver subjected to I/R, in light of the finding that MC deletion reduces the degree of liver injury. MCs are uniquely positioned around capillary vessels constituting pioneer part of the immune network, with regulatory functions in maintaining homeostasis and crucial pathological roles in vascular injury. Here, we further demonstrated that LSEC damage occurred initially via specific interactions with granule mediators within the liver, in turn, engaging machinery necessary for neutrophil infiltration, cytokine cascade as well as oxidative stress.

Gastrointestinal dysregulation is implicated in various liver pathological changes, such as non-alcoholic steatohepatitis [20], primary sclerosing cholangitis [21], and portal hypertension [22]. Liver I/R injury with evident LSEC impairment primarily occurs during the initial few hours after reperfusion. The mouse model used in our study with severe sinusoidal dilatation and confluent pericentral hepatocellular necrosis in liver was further characterized by gastrointestinal congestion and epithelial barrier damage, leading to modified homeostasis in response to inflammatory liver I/R injury. Following the inevitable histological injury to the gastrointestinal mucosa during hepatic I/R, the portal vein and arterial systems collect pathological products from the periphery of the digestive tract, which are eventually enriched and distributed in the liver.

MCs are tissue-dwelling immune cells predominantly located in the mucosal surface at the interface between the external and internal milieu, and the first to sense signaling through variable cell surface receptors (adenosine receptors, endothelin A receptors, and toll-like receptors) and intracellular receptors (nucleotide-binding oligomerization domain-containing proteins [NOD]-1 and NOD-2) [23]. Constitutive MCs in mammals are long-lived and pluralistic cells. Studies conducted on mice suggest that the phenotype and distribution of tissue MCs is determined by complex combinations of factors encountered by these cells and their progenitors in different tissue microenvironments [24]. Taking into account that routine H&E histochemistry performed on mucosal biopsies was unable to detect MCs and the inadequate evidence on MC localization, we combined multiple methods to determine distribution patterns of

© 2018 The Author(s). This is an open access article published by Portland Press Limited on behalf of the Biochemical Society and distributed under the Creative Commons Attribution License 4.0 (CC BY-NC-ND).

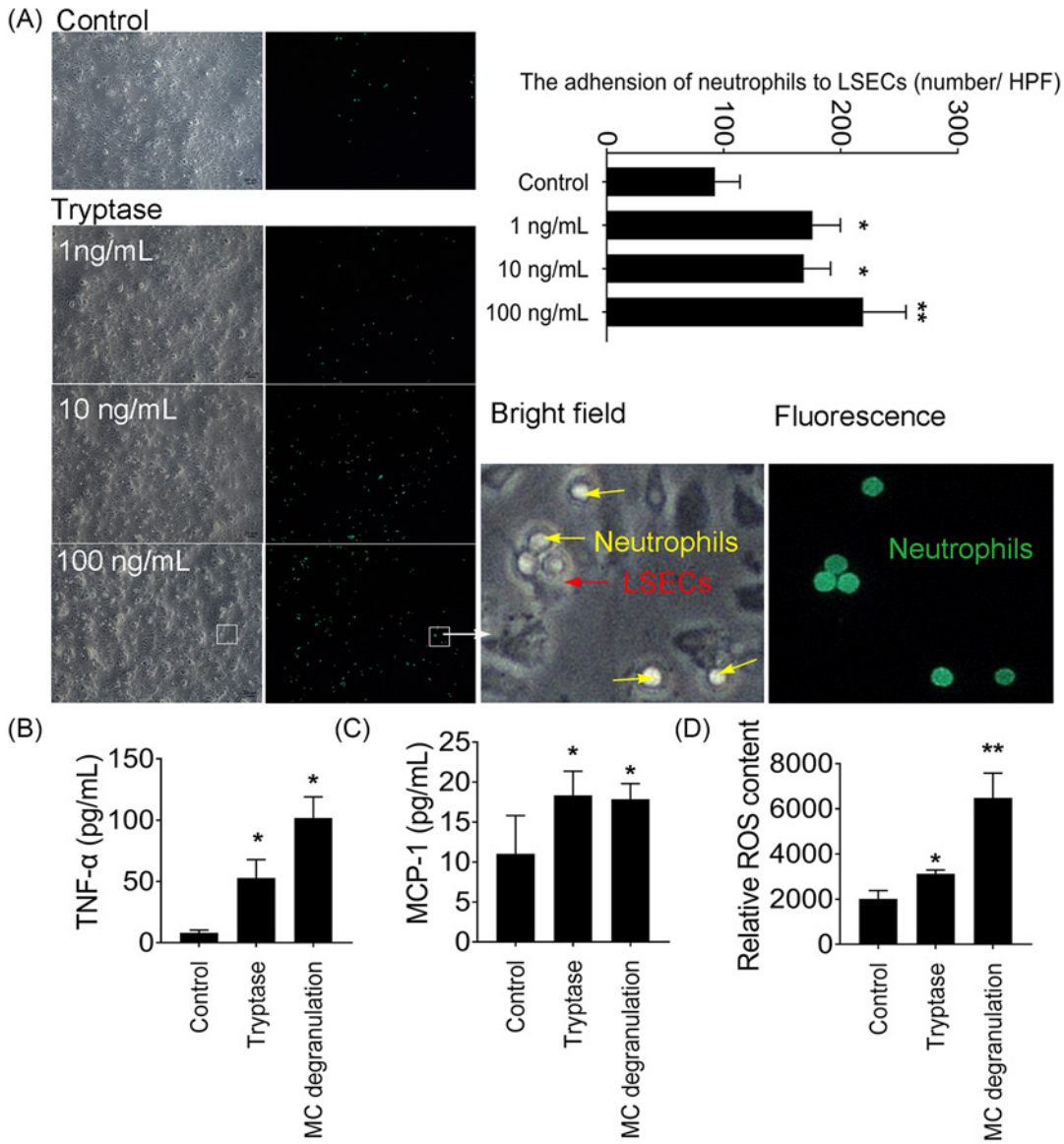

Figure 7. The granule component of MCs promotes neutrophil adhesion to LSECs and inflammation *in vitro*

(**A**) Analysis of adherent neutrophils to LSECs following tryptase treatment. Significant increase in (**B**) TNF-α, (**C**) MCP-1 in NPC culture supernatant, and (**D**) ROS content of NPCs stimulated by tryptase or MC granule. Data are presented as mean $\pm$ SEM. $^{*}P<0.05$ and $^{**}P<0.01$ for comparing with the corresponding control.

MCs in the liver and other organs of mice with the aid of the MC specific marker C-kit (CD117), tryptase, and FcεRI. As expected, murine parenchymal organs presented relatively low numbers of MCs. Regardless of whether or not the liver was subjected to I/R, MCs were always practically absent in murine liver. However, significant numbers of MCs were detected in close proximity to the gastrointestinal epithelium and mesenteric blood vessels, supporting potential regulatory roles of MC mediators infiltrating the capillaries. The therapeutic efficacy of MCs against IgE-dependent allergy [25] and parasite resistance [26], in part, due to their beneficial roles in innate and adaptive immunity, is well documented. However, when gastrointestinal MCs are challenged with a danger signal or perturbed in the tissue environment, they have the ability to shift from basal beneficial 'constitutive' to harmful 'reactive' forms [23].

Current knowledge on the function of MCs in I/R injury relates to degranulation, which correlates strongly with severity of organ injury [27]. Several methods are available for detection of MC degranulation, including toluidine blue staining, immunohistochemistry to determine specific granule contents, ELISAs to assess the release of granule proteins into serum, and electron microscope. Among these techniques, toluidine blue staining is the most commonly

© 2018 The Author(s). This is an open access article published by Portland Press Limited on behalf of the Biochemical Society and distributed under the Creative Commons Attribution License 4.0 (CC BY-NC-ND).

Clinical Science (2018) **132** 2241–2259
https://doi.org/10.1042/CS20180662

used. In the present study, we evaluated the specific granule contents of histamine and tryptase at different time-points to avoid bias. MC degranulation in stomach, intestine, and mesentery occurred rapidly in response to mucosal congestion. Both serum histamine and tryptase levels were increased during the ischemia period and peaked after 3 h reperfusion, suggesting roles in early liver pathology. Confirmatory evidence with our model was further obtained based on results of the correlation analysis between the degranulated gastrointestinal MC contents and markers of liver I/R damage, including *Suzuki's* score, serum ALT, and MDA levels. Our findings clearly indicated that the effects of gastrointestinal MCs during hepatic I/R should not be overlooked. To fully ascertain the effects of gastrointestinal MCs during the I/R process, experiments were conducted with $Kit^{W\text{-}sh/W\text{-}sh}$ and $Kit^{W\text{-}sh/W\text{-}sh}$ mice reconstituted with BMMCs from C57BL/6 mice. As expected, MC deficiency led to decreased necrotic and apoptotic cell death and preservation of normal liver function under conditions of I/R stress. These results were consistent with previous studies showing a detrimental function of MCs [9-11,27-30], especially in ischemia disease, and were supported by additional data on PARP activity, DNA fragmentation, and caspase 3/7 activity.

Liver capillaries are composed of LSECs located at a strategic interface between blood and parenchymal cells that presents a site for exchange of substances with the surrounding interstitial fluid playing crucial roles in liver homeostasis [31]. Liver I/R damage has been shown to be characterized by perturbations of molecules within the endothelium involved in survival and in other phenotypic changes of LSECs susceptible to the effects of digestive products [32]. Data from the present study showed that I/R stress strongly promotes LSEC death with typical features of apoptosis. Deletion of MCs led to significant reduction of cell death, consistent with changes in ICAM-1 and VCAM-1 expression levels in liver tissue. These two cell adhesion molecules are expressed on liver capillaries after activation of LSECs in specific pathological processes and play crucial roles in inflammatory injury, immune responses, and intracellular signaling events [33]. The degranulated contents derived from gastrointestinal MCs are enriched in the liver microcirculation system during I/R, in turn, orchestrating the LSEC death program and altering vascular reactivity to promote thrombosis. In fact, MCs are thought to play a relatively major role only in the early stages. During tissue inflammation, leukocyte–endothelial cell signal transduction mediated by adhesion molecules involves a series of sequential events including inflammatory or immune cell activation and migration in which the earliest activated effector cells are MCs, followed by secretion of performed mediators that facilitate the generation of specific pathological environments [34]. The time-course during which MCs play a leading role is limited. However, their potential activities in association with other cell types and convergence should not be overlooked.

Neutrophils are responsible, to a significant extent, for the physiopathological changes occurring during liver I/R injury under experimental conditions [35]. Based on the phenotype of LSEC death, we further demonstrated that one of the principal functional responses to I/R-induced MC activation in gastrointestinal and mesentery tissues was rapid recruitment of neutrophils in liver. Granule mediators released by MCs induce significant inflammatory pathology, both independently and in synergy with other cell-derived cytokines, and serve to orchestrate a complex immune response, exerting multiple effects on inflammatory cell recruitment. In addition to tryptase, chemokines and leukotrienes (in particular, LTC4) released by MCs also recruit neutrophils to inflamed tissues, which further potentiate damage [36]. TNF-α, an important contributor in neutrophil influx, is generated by several types of inflammatory cells. However, MCs are the only type known to presynthesize and store this cytokine in granules. Thus, MC-derived TNF-α is required for neutrophil infiltration during the early stages of liver injury. A previous study reported that MC activation produces the first of two peaks of TNF-α that augments neutrophil emigration in immune complex peritonitis [37]. Further experiments by our group revealed that the effects of MC degranulation contributing to neutrophil infiltration are also required for NET formation. NETs are extracellular scaffolds composed of nuclear DNA studded with granule proteins, histones, and cytoplasmic antimicrobials [38]. NET formation was recently implicated in exacerbating inflammatory cascades leading to augmentation of liver injury in response to endogenous damage-associated molecular pattern molecules in sinusoids [39]. Therefore, NET formation may present an important linking step through which MC degranulation induces liver damage.

Cytokine cascades as well as oxidative stress are the defining features of liver I/R, and their excessive generation by liver cells, LSECs, and immune cells results in proinflammatory extracellular milieu and tissue injury [2,40-42]. In addition, these molecules are involved in LSEC death and NET-promoting cascade. Consistent with these findings, the levels of a series of inflammatory factors and chemokines and oxidative stress markers were markedly increased upon gastrointestinal MC activation during liver I/R. Elevated levels of these molecules could promote adherence and migration of other circulating inflammatory cells to liver tissue. Among these mediators, TNF-α, IL-1, and IL-6 are directly released by activated MCs, and the chemokines CXCL1/CXCL2 act in concert with MCs to control the early stages of neutrophil infiltration during tissue inflammation [43]. Induction of high-output iNOS usually occurs in an oxidative environment. High levels of NO react with superoxides, leading to cell toxicity [44]. Our experiments further showed that excessive oxidative stress is induced by MC activation in parallel with increased liver neutrophil

© 2018 The Author(s). This is an open access article published by Portland Press Limited on behalf of the Biochemical Society and distributed under the Creative Commons Attribution License 4.0 (CC BY-NC-ND).

recruitment and LSEC death. These data strongly support the theory that the degree of initial injury by gastrointestinal MCs during liver I/R represents the major factor underlying pathologic development and highlights the need for early MC targeting therapeutic interventions in keeping with recent suggestions.

It is necessary to recognize certain limitations in our present study. One shortcoming is that the potential role of other possible confounding factors in the progression of liver damage cannot be ruled out. For example, increased permeability of the gastrointestinal mucosa can facilate intraluminal bacteria or bacterial products released into peritoneal cavity and circulatory system, thereby promoting the inflammatory damage of liver. Although MCs also enhance mucosa permeability, this is not a direct contribution of MC granule to liver damage [45]. Furthermore, increased numbers of activated gastrointestinal MCs alone do not give insight to proinflammatory capacity, as some evolutionarily conserved beneficial effect should be considered. Given that MCs in gastrointestinal system are unique with a high activity and maturity, the present study mainly relied on the intrinsic MCs in wild-type mice to explore their underlying action mechanism, even if we found the MCs exist in the liver of MC engraftment mice. At last, the relation between MCs and inflammatory damage may be also intrinsically dependent on the surgical procedures used for different clinical patients and experimental animal species. Thus, evidence of MC function obtained in the present study was limited to the exclusion of certain situations such as immune rejection during liver transplantation and metabolic factors in obese populations.

In summary, MCs occupy sentinel positions in tissues where many pathological factors attempt to attack and a special response typically begins [46,47]. Despite being allergic diseases, anaphylaxis and autoimmunity are mediated in a large part by MCs, and their precise roles in inflammatory injury require further investigation. By employing a novel c-Kit-independent mouse model, conditional MC deficiency and combining the features of MC distribution in a C57BL/6 mouse, we have provided preliminary *in vivo* evidence that gastrointestinal MCs are important contributors to the liver injury process following I/R, at least in part, through their granule functions in LSEC, to favor a more prominent acute neutrophil-driven inflammatory response involving NET formation, cytokine cascade, and oxidative stress. While major advances have been made in our understanding of the causes of liver I/R injury at the cellular and molecular levels, it appears that systemic factors, especially those participating in gastrointestinal pathology, also play a substantial role in disease development. Our findings have significant clinical relevance, as I/R is a common feature of many liver diseases, providing further support for the potential application of MC manipulation or drugs, such as Ketotifen and Sodium cromoglycate, which inhibit MC degranulation signaling in clinically relevant settings to protect against liver injury.

Clinical perspectives

- While major advances have been made in determining the causes of liver I/R injury at the cellular and molecular levels, systemic factors, in particular, those participating in gastrointestinal pathology, are also known to play a substantial role in liver disease development.
- MCs are tissue-resident immune cells abundant in the gastrointestinal system that perform diverse functions. These cells are closely related to the inflammatory injury process and inevitably activated in congested gastrointestinal mucosa caused by liver blockage.
- Here, we have demonstrated that gastrointestinal MC degranulation boosts the cycle of inflammatory damage during I/R via the liver blood supply system. Our findings have significant clinical relevance, supporting the theory that impairment of MC activity and/or decreasing MC numbers could serve as effective measures for protection against hepatic I/R injury.

Funding

This work was supported by grants from the National Natural Science Foundation of China [grant numbers 81470897 and 31741087].

Author Contribution

Z.H. conceived and performed most of the experiments. Y.L. and S.M. cultured and identified mast cells. Y.L., M.Y., Y.M., and C.M. performed some of the *in vivo* experiments. J.S., T.Y., and S.Z. performed the H&E staining and IHC. J.L. critically reviewed the manuscript and performed the data analysis. Z.H. and J.L. wrote the manuscript.

© 2018 The Author(s). This is an open access article published by Portland Press Limited on behalf of the Biochemical Society and distributed under the Creative Commons Attribution License 4.0 (CC BY-NC-ND).

Clinical Science (2018) **132** 2241–2259
https://doi.org/10.1042/CS20180662

Competing Interests

The authors declare no conflicts of interest.

Abbreviations

ALT, alanine aminotransferase; AST, aspartate aminotransferase; DCFH-DA, 5-chloromethyl-2,7-dichlorodihydrofluorescein diacetate acetyl ester; H&E, hematoxylin and eosin; HNE, 4-hydroxynonenal; HPF, high-powered field; ICAM-1, intercellular adhesion molecule 1; IFN-γ, interferon gamma; IL-9, interleukin 9; iNOS, inducible nitric oxide synthase; I/R, ischemia and reperfusion; MC, mast cell; MCP-1, monocyte chemoattractant protein 1; MDA, malondialdehyde; MPO, myeloperoxidase; NPC, non-parenchymal cell; PARP, poly (ADP-ribose) polymerase; ROS, reactive oxygen species; TNF-α, tumor necrosis factor alpha; VCAM-1, vascular cell adhesion molecule 1.

References

1 Zhai, Y., Busuttil, R.W. and Kupiec-Weglinski, J.W. (2011) Liver ischemia and reperfusion injury: new insights into mechanisms of innate—adaptive immune-mediated tissue inflammation. *Am. J. Transplant.* **11**, 1563–1569, https://doi.org/10.1111/j.1600-6143.2011.03579.x

2 Abu-Amara, M., Yang, S.Y., Tapuria, N., Fuller, B., Davidson, B. and Seifalian, A. (2010) Liver ischemia/reperfusion injury: processes in inflammatory networks—a review. *Liver Transpl.* **16**, 1016–1032, https://doi.org/10.1002/lt.22117

3 Theoharides, T.C., Alysandratos, K.D., Angelidou, A., Delivanis, D.A., Sismanopoulos, N., Zhang, B. et al. (2012) Mast cells and inflammation. *Biochimica. et Biophysica. Acta* **1822**, 21–33, https://doi.org/10.1016/j.bbadis.2010.12.014

4 Koda, K., Salazar-Rodriguez, M., Corti, F., Chan, N. Y.K., Estephan, R., Silver, R.B. et al. (2010) Aldehyde dehydrogenase activation prevents reperfusion arrhythmias by inhibiting local renin release from cardiac mast cells. *Circulation* **122**, 771, https://doi.org/10.1161/CIRCULATIONAHA.110.952481

5 Mattila, O.S., Pikkarainen, T.O. and Lindsberg, P.J. (2011) Cerebral mast cells mediate blood-brain barrier disruption in acute experimental ischemic stroke through perivascular gelatinase activation. *Stroke* **42**, 3600–3605, https://doi.org/10.1161/STROKEAHA.111.632224

6 Zheng, J., Wei, C.C., Hase, N., Shi, K., Killingsworth, C.R., Litovsky, S.H. et al. (2014) Chymase mediates injury and mitochondrial damage in cardiomyocytes during acute ischemia/reperfusion in the dog. *PLoS One* **9**, e94732, https://doi.org/10.1371/journal.pone.0094732

7 Krystel-Whittemore, M., Dileepan, K.N. and Wood, J.G. (2016) Mast cell: a multi-functional master cell. *Front. Immunol.* **6**, 620, https://doi.org/10.3389/fimmu.2015.00620

8 Kunder, C.A., John, A. L.S. and Abraham, S.N. (2011) Mast cell modulation of the vascular and lymphatic endothelium. *Blood* **67**, 65–73, https://doi.org/10.1182/blood-2011-07-358432

9 Tejada, T., Tan, L., Torres, R.A., Calvert, J.W., Lambert, J.P., Zaidi, M. et al. (2016) IGF-1 degradation by mouse mast cell protease 4 promotes cell death and adverse cardiac remodeling days after a myocardial infarction. *Proc. Natl. Acad. Sci. U.S.A.* **113**, 6949–6954, https://doi.org/10.1073/pnas.1603127113

10 Karhausen, J., Qing, M., Gibson, A., Moeser, A.J., Griefingholt, H., Hale, L.P. et al. (2013) Intestinal mast cells mediate gut injury and systemic inflammation in a rat model of deep hypothermic circulatory arrest. *Crit. Care Med.* **41**, e200, https://doi.org/10.1097/CCM.0b013e31827cac7a

11 Danelli, L., Madjene, L.C., Madera-Salcedo, I., Gautier, G., Pacreau, E., Mkaddem, S.B. et al. (2017) Early phase mast cell activation determines the chronic outcome of renal ischemia–reperfusion injury. *J. Immunol.* **198**, 2374–2382, https://doi.org/10.4049/jimmunol.1601282

12 Greenland, J.R., Xu, X., Sayah, D.M., Liu, F.C., Jones, K.D., Looney, M.R. et al. (2014) Mast cells in a murine lung ischemia-reperfusion model of primary graft dysfunction. *Respir. Res.* **15**, 95, https://doi.org/10.1186/s12931-014-0095-0

13 Shibamoto, T., Tsutsumi, M., Kuda, Y., Ohmukai, C., Zhang, W. and Kurata, Y. (2012) Mast cells are not involved in the ischemia-reperfusion injury in perfused rat liver. *J. Surg. Res.* **174**, 114–119, https://doi.org/10.1016/j.jss.2010.11.900

14 Yang, M.Q., Ma, Y.Y., Tao, S.F., Ding, J., Rao, L.H., Jiang, H. et al. (2014) Mast cell degranulation promotes ischemia–reperfusion injury in rat liver. *J. Surg. Res.* **186**, 170–178, https://doi.org/10.1016/j.jss.2013.08.021

15 Reitz, M., Brunn, M.L., Rodewald, H.R., Feyerabend, T.B., Roers, A. and Dudeck, A. (2017) Mucosal mast cells are indispensable for the timely termination of Strongyloides ratti infection. *Mucosal Immunol.* **10**, 481, https://doi.org/10.1038/mi.2016.56

16 Nastos, C., Kalimeris, K., Papoutsidakis, N., Tasoulis, M.K., Lykoudis, P.M., Theodoraki, K. et al. (2014) Global consequences of liver ischemia/reperfusion injury. *Oxid. Med. Cell. Longev.* **2014**, 906965, https://doi.org/10.1155/2014/906965 24799983

17 Gersch, C., Dewald, O., Zoerlein, M., Michael, L.H., Entman, M.L. and Frangogiannis, N.G. (2002) Mast cells and macrophages in normal C57/BL/6 mice. *Histochem. Cell Biol.* **118**, 41–49

18 Gaudenzio, N., Sibilano, R., Starkl, P., Tsai, M., Galli, S.J. and Reber, L.L. (2015) Analyzing the functions of mast cells in vivo using'mast cell knock-in'mice. *J. Vis. Exp.* **99**, e52753, https://doi.org/ 10.3791/52753

19 Lei, Y., Gregory, J.A., Nilsson, G.P. and Adner, M. (2013) Insights into mast cell functions in asthma using mouse models. *Pulm. Pharmacol. Ther.* **26**, 532–539, https://doi.org/10.1016/j.pupt.2013.03.019

20 Mouzaki, M., Comelli, E.M., Arendt, B.M., Bonengel, J., Fung, S.K., Fischer, S.E. et al. (2013) Intestinal microbiota in patients with nonalcoholic fatty liver disease. *Hepatology* **58**, 120–127, https://doi.org/10.1002/hep.26319

21 Grant, A.J., Lalor, P.F., Salmi, M., Jalkanen, S. and Adams, D.H. (2002) Homing of mucosal lymphocytes to the liver in the pathogenesis of hepatic complications of inflammatory bowel disease. *Lancet North Am. Ed.* **359**, 150–157, https://doi.org/10.1016/S0140-6736(02)07374-9

22 Villanueva, C., Colomo, A., Bosch, A., Concepción, M., Hernandez-Gea, V. and Aracil, C. (2013) Transfusion strategies for acute upper gastrointestinal bleeding. *N. Engl. J. Med.* **368**, 11–21, https://doi.org/10.1056/NEJMoa1211801

© 2018 The Author(s). This is an open access article published by Portland Press Limited on behalf of the Biochemical Society and distributed under the Creative Commons Attribution License 4.0 (CC BY-NC-ND).

23 Hamilton, M.J., Frei, S.M. and Stevens, R.L. (2014) The multifaceted mast cell in inflammatory bowel disease. *Inflamm. Bowel Dis.* **20**, 2364–2378, https://doi.org/10.1097/MIB.0000000000000142
24 Gurish, M.F., Pear, W.S., Stevens, R.L., Scott, M.L., Sokol, K., Ghildyal, N. et al. (1995) Tissue-regulated differentiation and maturation of a v-abl-immortalized mast cell-committed progenitor. *Immunity* **3**, 175–186, https://doi.org/10.1016/1074-7613(95)90087-X
25 Amin, K. (2012) The role of mast cells in allergic inflammation. *Respir. Med.* **106**, 9–14, https://doi.org/10.1016/j.rmed.2011.09.007
26 Mukai, K., Tsai, M., Starkl, P., Marichal, T. and Galli, S.J. (2016) IgE and mast cells in host defense against parasites and venoms. *Semin. Immunopathol.* , vol. 38, pp. 581–603
27 Strbian, D., Karjalainen-Lindsberg, M.L., Kovanen, P.T., Tatlisumak, T. and Lindsberg, P.J. (2007) Mast cell stabilization reduces hemorrhage formation and mortality after administration of thrombolytics in experimental ischemic stroke. *Circulation* **116**, 411–418, https://doi.org/10.1161/CIRCULATIONAHA.106.655423
28 Abonia, J.P., Friend, D.S., Austen, W.G., Moore, F.D., Carroll, M.C., Chan, R. et al. (2005) Mast cell protease 5 mediates ischemia-reperfusion injury of mouse skeletal muscle. *J. Immunol.* **174**, 7285–7291, https://doi.org/10.4049/jimmunol.174.11.7285
29 Bhattacharya, K., Farwell, K., Huang, M., Kempuraj, D., Donelan, J., Papaliodis, D. et al. (2007) Mast cell deficient W/Wv mice have lower serum IL-6 and less cardiac tissue necrosis than their normal littermates following myocardial ischemia-reperfusion. *Int. J. Immunopathol. Pharmacol.* **20**, 69–74, https://doi.org/10.1177/039463200702000108
30 Singh, M. and Saini, H.K. (2003) Resident cardiac mast cells and ischemia-reperfusion injury. *J. Cardiovasc. Pharmacol. Ther.* **8**, 135–148, https://doi.org/10.1177/107424840300800207
31 Stanger, B.Z. (2015) Cellular homeostasis and repair in the mammalian liver. *Annu. Rev. Physiol.* **77**, 179–200, https://doi.org/10.1146/annurev-physiol-021113-170255
32 Peralta, C., Jiménez-Castro, M.B. and Gracia-Sancho, J. (2013) Hepatic ischemia and reperfusion injury: effects on the liver sinusoidal milieu. *J. Hepatol.* **59**, 1094–1106, https://doi.org/10.1016/j.jhep.2013.06.017
33 Scoazec, J.Y. and Feldmann, G. (1994) The cell adhesion molecules of hepatic sinusoidal endothelial cells. *J. Hepatol.* **20**, 296–300, https://doi.org/10.1016/S0168-8278(05)80072-8
34 Muller, W.A. (2002) Leukocyte-endothelial cell interactions in the inflammatory response. *Lab. Invest.* **82**, 521, https://doi.org/10.1038/labinvest.3780446
35 Toledo-pereyra, L.H., Rodriguez, F.J. and Cejalvo, D. (1993) Neutrophil infiltration as an important factor in liver ischemia and reperfusion injury. *Transplantation* **55**, 1265–1271, https://doi.org/10.1097/00007890-199306000-00011
36 Okayama, Y. (2005) Mast cell-derived cytokine expression induced via Fc receptors and Toll-like receptors. *Chem. Immunol. Allergy* , vol. 87, pp. 101–110
37 Zhang, Y., Ramos, B.F. and Jakschik, B.A. (1992) Neutrophil recruitment by tumor necrosis factor from mast cells in immune complex peritonitis. *Science* **258**, 1957–1959, https://doi.org/10.1126/science.1470922
38 Cooper, P.R., Palmer, L.J. and Chapple, I.L. (2013) Neutrophil extracellular traps as a new paradigm in innate immunity: friend or foe? *Periodontol 2000* **63**, 165–197, https://doi.org/10.1111/prd.12025
39 Huang, H., Tohme, S., Al-Khafaji, A.B., Tai, S., Loughran, P., Chen, L. et al. (2015) Damage-associated molecular pattern–activated neutrophil extracellular trap exacerbates sterile inflammatory liver injury. *Hepatology* **62**, 600–614, https://doi.org/10.1002/hep.27841
40 Okaya, T. and Lentsch, A.B. (2003) Cytokine cascades and the hepatic inflammatory response to ischemia and reperfusion. *J. Invest. Surg.* **16**, 141–147, https://doi.org/10.1080/08941930390205782
41 Lentsch, A.B., Kato, A., Yoshidome, H., McMasters, K.M. and Edwards, M.J. (2000) Inflammatory mechanisms and therapeutic strategies for warm hepatic ischemia/reperfusion injury. *Hepatology* **32**, 169–173, https://doi.org/10.1053/jhep.2000.9323
42 Jaeschke, H. (2000) Reactive oxygen and mechanisms of inflammatory liver injury. *J. Gastroenterol. Hepatol.* **15**, 718–724, https://doi.org/10.1046/j.1440-1746.2000.02207.x
43 De Filippo, K., Dudeck, A., Hasenberg, M., Nye, E., van Rooijen, N., Hartmann, K. et al. (2013) Mast cell and macrophage chemokines CXCL1/CXCL2 control the early stage of neutrophil recruitment during tissue inflammation. *Blood* **121**, 4930–4937, https://doi.org/10.1182/blood-2013-02-486217
44 Beck, K.F., Eberhardt, W. O. L. F. G. A. N.G., Frank, S. T. E. F. A.N., Huwiler, A. N. D. R. E.A., Messmer, U.K., Muhl, H. et al. (1999) Inducible NO synthase: role in cellular signalling. *J. Exp. Biol.* **202**, 645–653
45 Peters, E.G., De Jonge, W.J., Smeets, B. J.J. and Luyer, M. D.P. (2015) The contribution of mast cells to postoperative ileus in experimental and clinical studies. *Neurogastroenterol. Motil.* **27**, 743–749, https://doi.org/10.1111/nmo.12579
46 Dahlin, J.S. and Hallgren, J. (2015) Mast cell progenitors: origin, development and migration to tissues. *Mol. Immunol.* **63**, 9–17, https://doi.org/10.1016/j.molimm.2014.01.018
47 Galli, S.J., Tsai, M., Wershil, B.K., Tam, S.Y. and Costa, J.J. (1995) Regulation of mouse and human mast cell development, survival and function by stem cell factor, the ligand for the c-kit receptor. *Int. Arch. Allergy Immunol.* **107**, 51–53, https://doi.org/10.1159/000236928

© 2018 The Author(s). This is an open access article published by Portland Press Limited on behalf of the Biochemical Society and distributed under the Creative Commons Attribution License 4.0 (CC BY-NC-ND).